Trafficking of Cholesterol to the ER is required for NLRP3 Inflammasome Activation

Marianne de la Roche[1,§], Claire Hamilton[1,§], Rebecca Mortensen[1], A. Arockia Jeyaprakash[2], Sanjay Ghosh[3,4], and Paras K. Anand[1,]*

[1]Infectious Diseases and Immunity, Department of Medicine, Imperial College London, London, W12 0NN, UK. [2]Wellcome Trust Centre for Cell Biology, Institute of Cell Biology, University of Edinburgh, Edinburgh, UK. [3]Department of Biochemistry, University of Cambridge, Cambridge, CB2 1QW, UK.

[§]These authors contributed equally to this work.

[4]Current address: Synthetic Biology Group, Institute of Bioinformatics and Applied Biotechnology, Biotech Park, Electronic City Phase I, Bengaluru 560100, India

***Correspondence should be addressed to:**
Paras K. Anand,
Infectious Diseases and Immunity,
Department of Medicine,
Imperial College London
Du Cane Road, The Commonwealth Building,
London, W12 0NN.
Tel: (020) 838 32063.
E-mail: paras.anand@imperial.ac.uk

Running Title: ER sterol levels modulate the NLRP3 inflammasome.

Keywords: NLRP3, NPC1, NLR, Inflammasome, ER, Cholesterol, trafficking, SREBP2

Abbreviations: NLR, NOD-like receptor; NPC1, Niemann-Pick C1; WT, wild-type.

Abstract

Cellular lipids determine membrane integrity and fluidity, and are being increasingly recognized to influence immune responses. Cellular cholesterol requirements are fulfilled through biosynthesis and uptake programs. In an intricate pathway involving the lysosomal cholesterol transporter NPC1, the sterol gets unequally distributed across intracellular compartments. By employing pharmacological and genetic approaches targeting NPC1, we reveal that blockade of cholesterol trafficking through the late-endosome/lysosome pathway blunts NLRP3 inflammasome activation. Altered cholesterol localization at the plasma membrane in *Npc1*$^{-/-}$ cells abrogated AKT-mTOR signaling by TLR4. However, the inability to activate the NLRP3 inflammasome was traced to perturbed cholesterol trafficking to the ER but not the plasma membrane. Accordingly, acute cholesterol depletion in the ER membranes by statins abrogated caspase-1 activation and IL-1β secretion, and ablated NLRP3 inflammasome assembly. By contrast, assembly and activation of the AIM2 inflammasome progressed unrestricted. Together, these studies reveal ER sterol levels as a metabolic rheostat for the activation of the NLRP3 inflammasome.

Introduction

The inflammasome is a multiprotein complex which plays critical roles in infectious, inflammatory, and autoimmune diseases. The NLRP3 inflammasome is the most characterised inflammasome in terms of diverse stimuli that are known to activate it. Activation of the NLRP3 inflammasome requires assembly of NLRP3 and caspase-1 bridged together through the adaptor protein ASC wherein caspase-1 undergoes autoproteolytic processing. Subsequently, active caspase-1 cleaves precursor forms of cytokines IL-1β and IL-18 which can then be secreted (Man and Kanneganti, 2015; Hamilton et al., 2017). Caspase-1 also cleaves gasdermin D making its N-terminal pore-forming domain active, leading to cell rupture (Kayagaki et al., 2015; Shi et al., 2015). Distinct exogenous, endogenous, and environmental stimuli are known to activate the NLRP3 inflammasome, implying that these stimuli do not bind NLRP3 directly but likely converge on shared upstream pathways. The mechanistic details of NLRP3 activation remain ambiguous.

Lipids are known to carry out diverse functions within cells, including being a major component of cell membranes, and as signalling messengers. Cholesterol is an essential lipid in mammalian cell membranes aiding varied functions, the most fundamental of which are membrane integrity and fluidity (Maxfield and Tabas, 2005). Levels of cholesterol in the cell are maintained through *de novo* synthesis in the endoplasmic reticulum (ER), and uptake of low-density lipoproteins (LDLs) derived from dietary cholesterol. Excess free cholesterol can be toxic to cells; thus, sterol homeostasis needs to be integrated by a combination of cholesterol uptake, biosynthesis, and efflux programs. At the subcellular level, cholesterol follows an intricate pathway in cells (Ikonen, 2008). Exogenously obtained LDL, bound to LDL receptor, is internalized at the plasma membrane and is transported through the endocytic pathway to the late-endosomes/lysosomes where cholesterol esters within the LDL core are hydrolyzed by acid lipases. Unesterified or free cholesterol translocates through the lysosomal cholesterol transporter Niemann-Pick C1 (NPC1) to other cellular sites such as the plasma

membrane and the ER. In the ER, cholesterol can be re-esterified permitting cytoplasmic storage in the form of lipid droplets.

Until recently, cholesterol has mostly been accepted to have an influence on immunity during pathologic conditions, such as in atherosclerosis (Fessler, 2016). However, evidence suggests that homeostatic lipid metabolism and trafficking directly regulates the inflammatory pathways in macrophages. For example, defective lipid trafficking in the absence of NPC1 leads to lysosomal storage disorder, Niemann-Pick disease (Platt et al., 2012). Mutations in the cholesterol efflux transporter, ABCA1, give rise to signs and symptoms of Tangier disease (Fasano et al., 2012). Similarly, perturbations in lipid metabolism contribute to several human pathologies including cardiovascular, obesity, and neurodegenerative diseases (Maxfield and Tabas, 2005). In addition to contributing to the pathogenesis of several diseases, cholesterol is also exploited by pathogens for their entry and proliferation within host cells. Several pathogens which lack the capacity for *de novo* sterol synthesis use cholesterol for their survival and replication by either increasing host lipid biosynthesis or redirecting cholesterol transport pathways (Ilnytska et al., 2013; Lauer et al., 2000; Coppens et al., 2000; Kaul et al., 2004; Carabeo et al., 2003). These studies suggest that reducing lipid synthesis may serve to limit nutrients available to pathogens thus benefitting host cells. Conversely, host cells need lipids for mounting a robust immune response to infection through conserved PRRs (Castrillo et al., 2003; York et al., 2015). Together, these studies lead to the hypothesis that lipid homeostasis is critical for an effective inflammatory response with implications for homeostatic lipid trafficking in both infectious and inflammatory diseases. Whether perturbations in homeostatic cholesterol trafficking pathway impact inflammasome activation remain unknown.

Here, by employing pharmacological and genetic tools, we demonstrate that selective perturbation of the cellular cholesterol trafficking in macrophages ablates inflammasome activation. Mechanistically, perturbed sterol trafficking in *Npc1*-deficiency leads to two distinct effects; altered PM cholesterol levels resulted in inhibition of the AKT-mTOR pathway, while reduced cholesterol trafficking to the ER blunted NLRP3 inflammasome assembly.

Accordingly, acute cholesterol depletion in the ER by statins decreased IL-1β secretion which could be restored by supplementing with exogenous cholesterol. Our findings thus implicate sterol synthesis and distribution as critical factors influencing the activation of the inflammasome, thereby coupling lipid homeostasis to innate immune signalling.

Results

Lysosomal sterol accumulation dampens inflammasome activation.

Homeostatic cholesterol trafficking is important as its distribution among subcellular organelles upholds vital housekeeping functions, and is critically dependent on lysosomal cholesterol transporter, NPC1. The lysosomal egress of cholesterol can be blocked by exposing cells to a cationic amphiphile and an androstenolone derivative, U18666a, which specifically targets NPC1 (Lu et al., 2015). To assess the effect of U18666a on cholesterol transport in our experiments, we first exposed bone-marrow-derived mouse macrophages (BMDMs) and immortalized BMDMs (iBMDMs) to the compound and examined cholesterol localization by staining with a naturally fluorescent polyene antibiotic, filipin. Filipin specifically binds to free cholesterol in biological membranes and can be excited by UV fluorescence. Filipin staining of control cells revealed diffused cholesterol staining throughout the cell **(Fig. S1)**. By contrast, and in conformity with previous studies in different cell types, exposure of BMDMs and iBMDMs to U18666a resulted in punctate structures reminiscent of lysosomes thus demonstrating lysosomal cholesterol accumulation **(Fig. S1a, b)** (Strauss et al., 2010; Maxfield and Wüstner, 2012). Notably, these punctate structures were completely absent in control cells. Furthermore, we observed no significant difference in total cholesterol levels in untreated, and LPS-treated cells in the presence or absence of U18666a suggesting that the elevated cholesterol accumulation in lysosomes is a result of altered sterol trafficking **(Fig. 1a)**. Together, these results established lysosomal cholesterol accumulation in mouse macrophages exposed to U18666a.

Next, to investigate the impact of cellular sterol trafficking on inflammasome activation, we exposed control and U18666a-treated BMDMs to LPS and ATP stimulation, a canonical ligand for activating the NLRP3 inflammasome. Activation of the NLRP3 inflammasome results in cleavage of pro-caspase-1 to its active form which subsequently processes precursor forms of cytokines IL-1β and IL-18 to their biologically active forms. Exposure of LPS-primed control cells to ATP resulted in robust caspase-1 activation which was significantly abolished in cells where cholesterol distribution was restricted to lysosomes **(Fig. 1b)**. In agreement, this was accompanied with significant reduction in IL-1β secretion compared to control cells **(Fig. 1c)**. To assess the specificity of this response, we next performed these experiments in BMDMs exposed to a range of U18666a concentrations followed by LPS and ATP stimulation. In confirmation with our above results, this resulted in a dose-dependent decrease in both caspase-1 activation and secretion of inflammasome-dependent cytokines IL-1β and IL-18 **(Fig. 1d, e, f)**. Finally, we confirmed these results with itraconazole, an antifungal drug which retards cholesterol trafficking from lysosomes. Similar to the results with U18666a, exposure to itraconazole resulted in reduced caspase-1 activation and IL-1β secretion **(Fig. S1c)**. The precise mechanism by which itraconazole blocks cholesterol trafficking is not known. However, previous reports established filipin colocalization with lysosomes but not PM, ER, and mitochondrial markers in endothelial cells exposed to the antifungal agent (Xu et al., 2010). Overall, these studies validated defective cholesterol trafficking as the cause of dampened inflammasome activation.

Activation of inflammasome is characterised by cell swelling and subsequent osmotic lysis in the form of pyroptotic cell death following gasdermin D cleavage (Kayagaki et al., 2015; Shi et al., 2015). In control cells primed with either LPS or Pam3, stimulation with ATP caused pyroptotic cell death. However, upon exposure to U18666a, cell death, and thus the secreted levels of cytosol-localized cell death marker, lactate dehydrogenase (LDH), were markedly diminished **(Fig. 1g-i)**. Overall these results demonstrate reduced caspase-1 activation, IL-1β and IL-18 secretion, and decreased pyroptosis when cellular cholesterol trafficking is inhibited.

Impaired cholesterol trafficking but not lysosomal dysfunction dampens inflammasome activation.

Because of their propensity to accumulate lipids, NPC1-mutant cells demonstrate impaired phagosome maturation (Huynh et al., 2008), autophagy (Sarkar et al., 2013), and defective NOD2-mediated microbial clearance (Schwerd et al., 2016). These studies prompted us to investigate whether lysosomal dysfunction in NPC1-mutant cells could account for defective inflammasome activation. To address this, we took advantage of v-ATPase inhibitor Bafilomycin A1 (Baf A1), which prevents phagosome-lysosome function, and chloroquine diphosphate (CQ), an inhibitor of lysosomal acidification. Exposure of LPS primed cells to either of these during the last 1h of priming resulted in comparable IL-1β secretion, dismissing reduced inflammasome activation as a secondary outcome of elevated lysosomal cholesterol accumulation **(Fig. 1j, k)**.

We next performed experiments to determine the role of priming in our assays. Activation of the NLRP3 inflammasome requires two signals. The first signal, which potentiates the NLRP3 inflammasome, is provided upon TLR ligation and results in the synthesis of pro-IL-1β and up regulation of NLRP3 expression (Anand et al., 2011a). This first signal (also known as the priming step) is dependent on the transcription factor NF-kB (Bauernfeind et al., 2009; Hornung and Latz, 2010). The second signal, which is more robustly provided by purinergic receptor $P2X_7$ agonist ATP, results in the assembly of NLRP3, caspase-1, and adaptor-protein ASC to form a multi-protein complex (Pelegrin and Surprenant, 2006). One potential explanation for defective inflammasome activation observed in experiments above could be the reduced priming of the NLRP3 inflammasome when sterol trafficking is perturbed. First, we demonstrate that the above results were not solely limited to TLR4 pathway, as exposure of U18666a-treated BMDMs to TLR2 agonist Pam3CSK4 followed by ATP stimulation also resulted in abolition of caspase-1 activation and IL-1β secretion **(Fig. S1d, e).** As expected, these results were entirely dependent on NLRP3 as *Nlrp3*$^{-/-}$ iBMDMs displayed blunted

caspase-1 activation and IL-1β production in cells exposed to inflammasome agonist nigericin **(Fig. S1f, g)**. Second, there was no reduction in the expression levels of NLRP3 and the secreted levels of the inflammasome-independent cytokine TNF-α, which are both transcriptionally-upregulated, and the adaptor ASC, when homeostatic cholesterol trafficking was abolished by pharmacological treatment in cells primed with either LPS or Pam3 **(Fig. 1d, S1d, h-j)**. On the contrary, a modest increase in NLRP3 and secreted levels of TNF-α were observed, likely because of elevation in TLR signaling upon cholesterol accumulation (Zhu et al., 2012, 2008; Yvan-Charvet et al., 2007). However, this did not directly correlate with transcript levels in our studies which were found comparable indicating an as yet unknown mechanism for post-transcriptional increase **(Fig. S1k-m)**. Taken together, these data excluded defective lysosomal function and priming as the reason for diminished NLRP3 activation.

Deficiency in *Npc1* abrogates NLRP3 inflammasome activation.

Cholesterol egress from lysosomes is directly dependent on sterol transporter, NPC1. Next, to validate our results in a genetic model, we generated *Npc1*-deficienct iBMDMs using CRISPR-Cas9 approach (see Methods, **Fig. S2**). Two independent clonal cell lines were obtained that showed deletion of variable lengths at the *Npc1* locus as validated by Sanger sequencing **(Fig. S2a, b)**. RT-qPCR analysis showed that, compared to WT cells, the *Npc1* mRNA levels in both clonal cell lines were significantly reduced **(Fig. S2c)**. Moreover, in agreement with the known function of NPC1, both mutant cell lines exhibited cholesterol accumulation in distinct punctate structures as revealed by filipin staining **(Fig. 2a)**. Thus, we concluded that CRISPR-Cas9 targeting resulted in deficiency of NPC1 activity and, therefore, the mutations are genuine loss-of-function alleles.

Exposure of LPS-primed wild-type cells to inflammasome agonist nigericin resulted in the maturation of 45 kDa pro-caspase-1 to 20 kDa active caspase-1. However, activation of caspase-1 was ablated in *Npc1*-deficient cells **(Fig. 2b)**. In agreement, IL-1β and IL-18 release

was also significantly abolished in *Npc1*-deficient cells **(Fig. 2c, d)**. As seen with the pharmacological inhibitor, there was a modest increase in NLRP3 expression in *Npc1*-deficient cells while secretion of the inflammasome-independent cytokine TNF-α remained unaffected **(Fig. 2b, e)**. Activation of cells with LPS+ATP reiterated defective caspase-1 activation and IL-1β release in *Npc1*-deficient cells while TNF-α secretion remained unaffected **(Fig. 2f-h)**. Furthermore, *Npc1*-deficient cells were remarkably protected from cell death **(Fig. 2i)**. These results thus establish both pharmacological and genetic knock-out of *Npc1* as valid approaches to block cholesterol lysosomal egress, and furthermore, implicate NPC1-dependent cellular sterol trafficking as pivotal for the activation of the NLRP3 inflammasome.

Lysosomal sterol efflux is not required for the activation of NLRC4 and AIM2 inflammasomes.

A diverse array of signals is known to activate the NLRP3 inflammasome. In contrast, ligands that activate the NLRC4 and AIM2 inflammasomes are well defined. NLRC4 inflammasome is triggered by the recognition of cytosolic flagellin and components of the bacterial secretion system by upstream NAIP family members (Amer et al., 2006; Kofoed and Vance, 2011; Zhao et al., 2011). AIM2 inflammasome, in contrast, is activated by recognition of dsDNA of ~80bp in length (Jin et al., 2012). We next tested whether the requirement for homeostatic cholesterol transport is specific to the activation of the NLRP3 inflammasome. First, we tested whether lysosomal sterol accumulation affects NLRC4 inflammasome activation by infecting macrophages with *Salmonella typhimurium.* Unlike NLRP3, caspase-1 activation by the NLRC4 inflammasome remained unaffected in cells where NPC1 was pharmacologically blocked **(Fig. 3a)**. In agreement, *Npc1*$^{-/-}$ cells also demonstrated caspase-1 activation and IL-1β secretion comparable to that observed in infected WT cells **(Fig. 3b, c)**. We next evaluated whether the DNA sensing AIM2 inflammasome is affected by sterol lysosomal compartmentalization. To evaluate this, WT cells (in the presence or absence of U18666a) and *Npc1*$^{-/-}$ cells were transfected with poly(dA:dT). Western blotting revealed no impact on

caspase-1 activation upon poly(dA:dT) transfection when lysosomal egress of cholesterol was blocked **(Fig. 3d)**. These results demonstrate that sterol lysosomal compartmentalization uniquely affects the NLRP3 inflammasome.

Cholesterol compartmentalization dampens Gasdermin D -mediated ASC-independent pyroptosis following NLRC4 inflammasome activation

Activation of the inflammatory caspases (including caspase-1) results in the cleavage of gasdermin D (GSDMD) to remove the auto-inhibitory C-terminal fragment. The resulting active N-terminal cleavage product oligomerizes to form membrane pores to trigger pyroptosis (Shi et al., 2015; Kayagaki et al., 2015; Ding et al., 2016). Previous studies demonstrated that induction of pyroptosis, as demonstrated by LDH release, during NLRC4 inflammasome activation by *Salmonella*, is ASC-independent but caspase-1-dependent. Surprisingly, NLRC4-dependent pyroptosis progressed in the absence of caspase-1 auto-proteolysis (Broz et al., 2010). We therefore took advantage of these studies to assess whether sterol lysosomal efflux influenced the induction of ASC-independent pyroptosis. As observed above, blockade of cholesterol transport in WT cells did not inhibit caspase-1 activation by *Salmonella* infection **(Fig. 3a)**. Accordingly, cleavage of GSDMD was also similar when NPC1 was pharmacologically blocked in WT cells **(Fig. 3e)**. In agreement with previous studies, pyroptosis, and thus GSDMD N-terminal fragment, was not observed in *casp-1/11*$^{-/-}$ cells but was cleaved in *Asc*$^{-/-}$ cells comparably to WT cells **(Fig. 3e)**. Surprisingly, *Asc*$^{-/-}$ cells treated with U18666a exhibited reduced GSDMD cleavage suggesting a role for homeostatic cholesterol transport in pyroptosis only in the absence of ASC **(Fig. 3e)**. By contrast, cholesterol accumulation had no effect on GSDMD cleavage either in U18666a-treated or in *Npc1*$^{-/-}$ cells following AIM2 inflammasome activation by poly(dA:dT) transfection **(Fig. 3d)**. Conversely, GSDMD cleavage was reduced following NLRP3 inflammasome activation with both LPS + ATP and Pam3 + ATP, mirroring the effects seen on caspase-1 activation **(Fig. 3f, g)**. These data thus suggest that cholesterol lysosomal egress is required for ASC-

independent pyroptosis following NLRC4 activation. However, pyroptosis following activation of the AIM2 inflammasome is not affected.

Cholesterol supplementation restores inflammasome activation

Variation in the levels of cholesterol and other lipids within the cell are sensed by master transcriptional regulators SREBP1 and SREBP2 which, respectively, regulate fatty acid and cholesterol biosynthesis (Horton et al., 2002). A feedback mechanism tightly regulates cholesterol *de novo* biosynthesis to maintain homeostatic levels. Cholesterol depletion triggers ER resident sterol cargo protein SCAP to escort SREBP2 to the Golgi where the precursor is cleaved to activate cholesterogenic genes. By contrast, in cholesterol replete cells, conformational change in SCAP promotes insulin-induced gene (INSIG)-mediated retention of SREBP2 in the ER.

Low ER cholesterol is an established trigger for SREBP2 activation. Although the movement of cholesterol from the NPC1 compartment to the PM and to the ER is defective in cells lacking functional NPC1 (Sugii et al., 2003; Cruz et al., 2000), the total cholesterol levels were not considerably elevated when NPC1 was pharmacologically blocked **(Fig. 1a).** To investigate this further, we quantified SREBP2 targets HMG-CoA synthase (*Hmgcs1*) and HMG-CoA reductase (*Hmgcr*) in LPS primed cells, and the transcript levels were significantly down-regulated in *Npc1*$^{-/-}$ cells **(Fig. S2d-f)**. Intriguingly, the expression of *Srebp2* was also reduced in *Npc1*-deficient cells thereby reconfirming previous studies that SREBP2 autoregulates its own mRNA expression (Sato et al., 1996). The decreased expression of SREBP2-dependent genes likely also results in reduced nuclear localization of the mature protein as correlation has been observed in other studies (Repa et al., 2000; Im et al., 2011). The levels of *Srebp2* and the target gene *Hmgcs1* were elevated in control *Npc1*$^{-/-}$ cells **(Fig. S4a)**.

SREBP-dependent lipogenesis is regulated by mTORC1, a master regulator of cellular metabolism (Porstmann et al., 2008; Peterson et al., 2011). By evaluating the phosphorylation

of ribosomal protein p70 S6 kinase 1 (S6K1), a direct mTOR substrate, we investigated the upstream pathway that modulates SREBP2 in our study. *Npc1*$^{-/-}$ and U18666a exposed cells displayed reduced phosphorylation of S6K1 and the upstream mTOR regulator serine/threonine protein kinase AKT (protein kinase B) in cells exposed to LPS in a time-course experiment **(Fig. S3)**. The decrease in the activation of AKT-mTOR pathway is likely a result of disorganized lipid raft micro-domains in the PM of *Npc1*$^{-/-}$ cells (Vainio et al., 2005; Simons and Toomre, 2000). Accordingly, *Npc1*$^{-/-}$ cells exhibited reduced PM cholesterol levels as measured by its' susceptibility to cholesterol oxidase **(Fig. S4b)**. Indeed, reduction in PM cholesterol in wild-type cells by methyl-β-cyclodextrin (MCD) treatment resulted in reduced mTOR activity (unpublished results). Furthermore, inhibition of mTOR by selective inhibitor Torin1 significantly decreased the expression of *Srebp2* and the target genes *Hmgcs1* and *Hmgcr* **(Fig. S2g-i)**. The regulation of SREBP2 by mTOR is well established and involves the phosphatidic acid phosphatase, lipin-1, which functions at several steps to control SREBP activity (Peterson et al., 2011). These results demonstrate reduced mTOR- and SREBP2-dependent lipogenesis in *Npc1*$^{-/-}$ cells following LPS stimulation.

Since our observations above suggested overall reduction in cholesterol in sub-cellular organelles, we reasoned that supplementation with exogenous cholesterol should restore inflammasome activity. To conduct these experiments, methyl-β-cyclodextrin (MCD)-solubilized cholesterol was added to LPS-primed cells cultured in serum-free medium 1h before ATP treatment to assess only the effects on the second signal of inflammasome activation. Remarkably, supplementation with soluble cholesterol restored inflammasome activation in cells where lysosomal egress of cholesterol was pharmacologically blocked, resulting in both distinct increase in caspase-1 cleavage and IL-1β secretion **(Fig. 4a, b)**. The addition of cholesterol/MCD complex to LPS primed cells in the absence of ATP was insufficient to activate the inflammasome while exposure to alum resulted in abundant IL-1β secretion suggesting the crystal-independent nature of cholesterol/MCD-induced NLRP3 inflammasome **(Fig. 4b, c)**. Similarly, cholesterol/MCD, by itself, was insufficient at providing

'signal 1' in the absence of LPS **(Fig. 4a, b)**. *Npc1*$^{-/-}$ cells supplemented with exogenous cholesterol/MCD reiterated elevated IL-1β secretion **(Fig. 4d)**. Also, this response appeared to be concentration dependent, with the optimal concentration of cholesterol peaking at around 15 µg/ml **(Fig. 4e, f)**. Collectively, these results demonstrate that replenishment with soluble cholesterol in cells with non-functional NPC1 restores caspase-1 activation and IL-1β production.

Cholesterol depletion in the ER membranes abrogates caspase-1 activation and IL-1β secretion.

We next investigated the sub-cellular site to which the cholesterol must localize to for optimal inflammasome activity. To address this, we first focussed on the plasma membrane which is the largest pool of cholesterol in the cell where it makes up 50-60% of total lipids (Ridsdale et al., 2006). To measure the contribution of PM, we took advantage of a routinely used cholesterol extraction agent MCD to deplete PM cholesterol from cells cultured in lipoprotein-deficient serum. We recognised from our experiments above that changes to the PM cholesterol affect AKT-mTOR signaling. Therefore, to eliminate the involvement of other pathways and to specifically address the role of PM cholesterol in the second step of inflammasome activation, we exposed LPS-primed BMDMs to MCD only for 30 min before ATP stimulation. We reasoned that restricted exposure to MCD would affect only the PM cholesterol while retaining the architecture of other cellular cholesterol pools (Ridsdale et al., 2006). As expected, exposure to MCD resulted in reduction in total cholesterol levels by approximately 60% **(Fig. 5a)**. However, subsequent treatment with ATP did not affect caspase-1 activation or IL-1β release **(Fig. 5b, c),** excluding any role for PM cholesterol in inflammasome activation.

The transport of cholesterol from the NPC1 compartment to the ER is blunted in cells lacking functional NPC1 (Sugii et al., 2003; Cruz et al., 2000). In agreement, *Npc1*$^{-/-}$ cells exhibited diminished levels of esterified cholesterol **(Fig. 5d)**. Therefore, we next examined the role of

cholesterol in the ER membranes which are cholesterol poor with only 3-6% of total lipids. To specifically deplete cholesterol in the ER, we took advantage of the fact that cells grown in lipoprotein-deficient serum depend entirely on endogenous cholesterol synthesis to support growth (Ridsdale et al., 2006). We therefore exposed LPS-primed cells to statins, specific inhibitors of cholesterol biosynthetic pathway, to cause acute cholesterol depletion of the ER pool. Statin treatment initially decreases cholesterol specifically in the ER membranes, therefore, we restricted statin treatment to only 1h before ATP stimulation. In agreement with its' function, exposure of control cells to fatostatin resulted in reduced expression of SREBP2 and the target genes **(Fig. S4c).** Inflammasome activation in cells exposed to fatostatin resulted in significantly reduced IL-1β secretion **(Fig. 5e)**. Similarly, treatment with lovastatin and mevastatin, which target HMG-CoA reductase, the rate limiting enzyme of cholesterol synthesis, also resulted in reduced caspase-1 cleavage and IL-1β secretion upon NLRP3 activation **(Fig. 5f, g)**. Conversely, addition of either cholesterol/MCD or mevalonate, the direct product of HMG-CoA reductase, to the media of statin-exposed cells restored IL-1β secretion **(Fig. 5h, S4d)**. Statin treatment, however, affected only the NLRP3 inflammasome. Exposure of cells grown in lipoprotein-deficient media to lovastatin during the last 1h of AIM2 inflammasome activation by poly(dA:dT) transfection did not affect caspase-1 activation **(Fig. 5i)**. Consequently, secretion of IL-18 was also comparable regardless of the presence of lovastatin during poly(dA:dT) transfection **(Fig. 5j)**. As expected, the secretion of IL-18 and IL-1β was significantly diminished during LPS and ATP stimulation **(Fig. 5j, k)**. These observations unequivocally demonstrate that ER cholesterol is required for the NLRP3 inflammasome activation.

ER cholesterol depletion blunts ASC-dependent inflammasome assembly.

Activation of inflammasome and IL-1β secretion is critically dependent on the assembly of the supramolecular complex containing NLRP3, ASC, and caspase-1. The assembly of this complex is quite elaborate and requires the release to the cytoplasm of mitochondria-

associated ER membranes (MAMs) - localized NLRP3 which, in the presence of the activating stimuli, nucleates the ASC filament, believed to be a major determinant for inflammasome assembly and the downstream cellular functions of inflammasomes. ASC, a bipartite protein composed of a PYD and a CARD domain, acts as an adaptor protein linking the PYD-containing NLRP3 to the CARD-containing caspase-1 through homotypic interactions. Upon receptor activation, ASC oligomerizes to form the so-called ASC speck, a macromolecular complex which is ~1-2 μm in diameter. Under resting conditions, ASC is present diffusely throughout the cytoplasm. Stimulation of the NLRP3 inflammasome with LPS+ATP was sufficient to assemble the inflammasome resulting in ASC speck formation in control WT cells **(Fig. 6a)**. However, ASC speck formation was significantly abolished both in *Npc1*$^{-/-}$ cells and in cells where NPC1 was pharmacologically blocked by U18666a **(Fig. 6a, b)**. We next independently verified if ER cholesterol depletion by statin treatment could also blunt the assembly of the NLRP3 inflammasome. As before, we grew BMDMs in lipoprotein-deficient media and depleted ER cholesterol by exposing LPS-primed cells to lovastatin for 1h before ATP stimulation. In response to NLRP3 agonist ATP, control cells revealed expected levels of ASC speck formation. However, percentage of cells showing ASC specks was significantly reduced in samples treated with lovastatin **(Fig. 6c, e)**. Similarly, control cells exposed to AIM2 agonist poly(dA:dT) demonstrated ASC speck formation. However, in contrast to the NLRP3 inflammasome, ER cholesterol depletion by exposure to lovastatin during the last 1h of poly(dA:dT) transfection did not influence the assembly of the AIM2 inflammasome **(Fig. 6d,e)**. These results thus suggest that NLRP3 complex formation is distinctly regulated by ER cholesterol pool.

NLRP3 recruitment to ASC is diminished in *Npc1*-deficient cells.

Biochemical evidence suggests that NLRP3 is mainly localized on MAMs, thus positioning NLRP3 in close proximity to mitochondria-released effectors many of which are known to activate the NLRP3 inflammasome (Lupfer et al., 2014, 2013; Nakahira et al., 2011; Zhou et

al., 2011; Iyer et al., 2013; Wang et al., 2013; Gurung et al., 2015). On the contrary, the majority of the ASC is found in the cytoplasmic fraction before inflammasome activation although a minor portion of ASC is found associated with the ER fraction (Zhou et al., 2011). However, the fully active inflammasome complex is mostly cytoplasmic suggesting the requirement of additional steps in the activation of the inflammasome (Wang et al., 2013; Zhou et al., 2011). Intriguingly, the described distribution of the activating receptor is specific to the NLRP3 inflammasome while localization of non-NLRP3 inflammasomes remains less characterized. We next tested the localization of NLRP3. In agreement with previous studies, control LPS-primed cells exhibited a fraction of NLRP3 close to MAMs as revealed by double labelling with ER maker calreticulin **(Fig S5a)**. Upon subsequent exposure to ATP, NLRP3 was found strongly associated to ASC in WT cells **(Fig. 7a, b)**. However, this was significantly diminished in *Npc1*$^{-/-}$ cells where NLRP3 and ASC were both found diffusely localized throughout the cell **(Fig. 7c, d)**. Quantitative analysis revealed a signification reduction in NLRP3 association with ASC in *Npc1*-deficient cells **(Fig. 7e)**. As expected, the assembled inflammasome did not show significant association with ER while mitochondria were found in close vicinity **(Fig. S5b)**. However, in agreement with other studies, ASC speck was found associated with mitochondria and ER in a fraction of cells. Our studies thus suggest that ER cholesterol is pivotal for recruitment of NLRP3 to ASC and thus full activation of the NLRP3 inflammasome. Overall, our data suggest that cholesterol acts as a rheostat to modulate NLRP3 activity and thus these studies may be useful to develop novel therapeutics to treat NLRP3-related disorders.

Discussion

Our studies demonstrate that homeostatic sterol trafficking and distribution provides an appropriate intracellular milieu for the activation of the NLRP3 inflammasome. Pharmacological or genetic blockade of NPC1 blunted NLRP3 inflammasome activation resulting in reduced caspase-1 activation and IL-1β secretion in response to NLRP3 agonists.

Remarkably, cellular cholesterol trafficking uniquely affects the NLRP3 inflammasome while activation of the NLRC4 and AIM2 inflammasomes remained unimpeded. Further mechanistic studies suggested that cholesterol trafficking to the ER licenses the NLRP3 inflammasome activation. In agreement, acute depletion of the ER cholesterol pool by statin treatment abrogated the assembly and activation of the NLRP3 inflammasome.

A previous study associated inflammasome activation to dietary cholesterol (Progatzky et al., 2014). The authors observed an increase in the accumulation of myeloid cells in the intestine of zebrafish that were fed a high cholesterol diet, which was found to be dependent on cholesterol uptake by plasma membrane localized NPC1-like 1 (NPC1L1). Inhibitors of both NPC1L1, and inflammasome components, reduced the accumulation of myeloid cells. This study thus provided evidence that cholesterol uptake by NPC1L1 is able to activate the inflammasome (i.e. provide 'signal 2'). However, inflammasome activation by cholesterol uptake was restricted to intestinal epithelial cells with no role identified for haematopoietic cells (Progatzky et al., 2014). In agreement, NPC1L1 is expressed predominately in the gastrointestinal tract, whereas lysosomal NPC1 is more abundantly expressed in a wide variety of cells and tissues (Altmann et al., 2004). Our study signifying the role of macrophage sterol trafficking in NLRP3 activation thus unravels distinct mechanisms of NPC1 and NPC1L1 in modulating inflammasome in discrete cell types.

Previous studies have highlighted a role for cholesterol in NLRP3 inflammasome activation during atherosclerosis (Duewell et al., 2010; Sheedy et al., 2013; Rajamäki et al., 2010; Freigang et al., 2011). Mice fed atherogenic diet displayed 'cholesterol crystal' formation as early as two weeks in atherosclerotic lesions which correlated with macrophage recruitment (Duewell et al., 2010). The inflammasome activation in the above studies was dependent on macrophage lysosomal rupture and subsequent cathepsin B release into the cytoplasm following accumulation of 'cholesterol crystals' within the degradative organelle (Hornung et al., 2008). Whether cellular cholesterol trafficking directly impacts inflammasome activation remained unknown. Our data demonstrate that blockade of cholesterol trafficking through

NPC1 dampened NLRP3 inflammasome which could be restored by addition of exogenous cholesterol. These findings are in agreement with a recently published study in which exogenous cholesterol was shown to activate the AIM2 inflammasome (Dang et al., 2017). However, in their study, cells were exposed to cholesterol/MCD for 8h which eventually resulted in mitochondrial dysfunction and increased cytosolic mtDNA content. Thus, inflammasome activation in their research was dependent on DNA sensor AIM2. However, we exposed macrophages for only 1h with cholesterol/MCD followed by canonical NLRP3 stimuli, ATP, thereby implicating a role for NLRP3 inflammasome in our study. Together, these studies demonstrate that cholesterol function in distinct organelles modulates different inflammasomes.

In cells lacking functional NPC1, the movement of cholesterol from the NPC1 compartment to the ER and to the PM is defective (Sugii et al., 2003; Wojtanik and Liscum, 2003). In agreement, *Npc1*$^{-/-}$ cells exhibited both reduced levels of esterified cholesterol and decreased sensitivity to cholesterol oxidase. Thus, *Npc1*-deficiency alters plasma membrane order and composition, thereby affecting discrete cholesterol-dependent signalling networks localized in lipid rafts (Simons and Ehehalt, 2002). This is most likely the reason for both the reduced activation of AKT- mTOR - SREBP2 axis and a modest increase in *Npc1*$^{-/-}$ cells of the NLRP3 expression, the latter agreeing with elevated TLR signalling when cellular sterol efflux is blocked (Zhu et al., 2008). However, it is difficult to reconcile these data at the moment considering that contrasting responses were observed with signal emanating from the same TLR4 receptor. Though, our data would imply an unidentified post-transcriptional mechanism for enhanced TLR responses upon cholesterol accumulation.

We found a key role for ER cholesterol pool in inflammasome activation while deviation in the PM cholesterol levels did not affect caspase-1 activation and IL-1β secretion. Our model suggesting a significant role for ER cholesterol agrees with previous studies **(Fig. 7)**. Inhibition of SREBP processing by 25-hydroxy cholesterol results in reduced IL-1β production (Reboldi et al., 2014a). Likewise, BMDMs lacking SCAP, which chaperones SREBP2 to the Golgi for

processing, exhibit reduced caspase-1 activation and IL-1β expression (Reboldi et al., 2014b). Under resting conditions, NLRP3 is mainly localized on MAMs (Zhou et al., 2011) which are cholesterol-poor and sensitive to changes in cholesterol levels. NLRP3 release from MAMs is necessary to oligomerize with cytoplasmic ASC when a second signal is available (Zhou et al., 2011; Zhang et al., 2017; Wang et al., 2013). ER is known to influence innate immune signalling but the underlying mechanisms remain unclear (Toulmay and Prinz, 2011; Misawa et al., 2017). Together with our data, this raises an intriguing possibility that ER lipid composition might play a direct or indirect function in modulating immune responses, including the activation of inflammasome.

We observed a significantly reduced association of NLRP3 and cytoplasmic ASC in *Npc1*$^{-/-}$ cells suggesting that cholesterol likely provides fluidity to the ER membranes to allow NLRP3 release and subsequent assembly of an active inflammasome. However, at this time, it is difficult to rule out the additional roles of ER cholesterol upstream of the inflammasome assembly formation and NLRP3 activation. For example, ER cholesterol may be required to provide the necessary conformation to NLRP3 to sense the activating effectors. Similarly, ER cholesterol might also enable NLRP3 association with ASC by allowing the extension of the ER tubules prior to the dissociation of the complex from the ER. In agreement with this, a fraction of cells displayed ASC specks that exhibited association with calreticulin (not shown). Furthermore, in the latter scenario, cholesterol might also have a direct role in inflammasome assembly. It will be interesting to dissect the precise roles of ER cholesterol in inflammasome assembly and activation in future studies. Overall, our studies reveal an essential requirement for sterol trafficking to the ER for the activation of the NLRP3 inflammasome. The results presented here may provide clues to develop novel treatment avenues for diseases where dysregulated lipid metabolism is the underlying factor.

Materials and Methods

Ethics Statement

Experiments were performed in accordance with the Animals (Scientific Procedures) Act 1986 and were approved by Imperial College Animal Welfare and Ethical Review Body (AWERB) and the UK Home Office.

Bone-marrow derived macrophage culture

C57BL/6 mice were obtained from Charles River, UK. Bone-marrow cells were isolated from 6-10-week-old mouse femurs and tibias as previously described (Anand et al., 2011b) and allowed to differentiate into macrophages in Dulbecco's Modified Eagle Medium (DMEM) containing 10% heat-inactivated fetal bovine serum (FBS), 1% penicillin/streptomycin, 1% HEPES, and 30% conditioned media from L929 fibroblasts. The cells were allowed to differentiate for 5-6 days at 37 °C. After being harvested, cells for some experiments were grown in media containing 5% lipoprotein-deficient serum as indicated. Wild-type (WT), *Nlrp3*$^{-/-}$*, Asc*$^{-/-}$*, and Casp1/11*$^{-/-}$ immortalised BMDMs (iBMDMs) were kindly provided by Katherine Fitzgerald, Thirumala-Devi Kanneganti, and Clare Bryant. iBMDMs were cultured in DMEM containing 10% FBS, 1% penicillin/streptomycin, and 10% L929 conditioned medium in 10 cm^2 tissue culture plates. Cells were grown until confluent and split every 2-3 days.

Cell stimulations

Primary BMDMs and iBMDMs were seeded in 24-, 12- or 6-well plates at a density of 0.5 x 10^6, 1 X 10^6 or 2 X 10^6 cells per well, respectively. Experiments with U18666a (662015, Calbiochem) were optimized in different cell types so as to block lysosomal efflux of cholesterol and achieve absolute lysosomal accumulation. Primary BMDMs exposed to U18666a displayed lysosomal cholesterol accumulation at 48h while in iBMDMs, sufficient cholesterol accumulation was observed by 24h **(Fig. S1)**. Where used, cells were exposed to Torin1 (CAY10997, Cayman Chemical) for 3h, Bafilomycin A1 (Sigma) and Chloroquine diphosphate (Sigma) at the indicated concentrations for 1h before ATP stimulation.

Inflammasome activation assays

For NLRP3 activation, cells were primed with 500 ng/ml of either lipopolysaccharide (LPS, tlrl-pbslps, Invivogen) or Pam3 (tlrl-pms, Invivogen) for 4 hours followed by addition of either 5 mM ATP (A6419, Sigma) or 20 nM nigericin (4312, Tocris) for 45 minutes. Cell images were taken using a light microscope following addition of either ATP or nigericin. Alum was used at 1 mg/ml for 16h in LPS-primed cells grown in complete media. For NLRC4 activation, cells were infected with *Salmonella typhimurium* strain SL1344 (kind gift from Jorge Galan and Avinash Shenoy) at a MOI of 2 for approximately 4h. For AIM2 inflammasome activation, cells grown in 24-well plates were transfected with 1 μg of poly(dA:dT) using Lipofectamine 2000 (Invitrogen) according to manufacturer's recommendations. Following each condition, cell supernatants were collected and immediately frozen for cytokine analysis and the cell lysates were harvested in RIPA lysis buffer for immunoblot analysis.

Generation of CRISPR-Cas9 targeting constructs

The CRISPR design tool (http://crispr.mit.edu) was used to identify two candidate gRNA sequences (compatible with *S. pyogenes* Cas9 and its protospacer adjacent motif (PAM, 5′-NGG)) near the 5' region of the mouse *Npc1* gene (NM_008720). 5′-phosphorylated oligonucleotides containing the gRNA sequences (underlined) and BbsI adapter are as follows: gRNA1 (5'-CACCG<u>CGACCCGAGCGTCGCGGCAC</u>-3' and its reverse complement 5'-AAAC<u>GTGCCGCGACGCTCGGGTCG</u>C-3'), gRNA2 (5'-CACCG<u>TCGGAACCGGCGCCTGACCA</u>-3' and its reverse complement 5'-AAAC<u>TGGTCAGGCGCCGGTTCCGA</u>C-3'). The gRNA1 and gRNA2 oligonucleotides were annealed and ligated into pSpCas9(BB)-2A-GFP plasmid (Addgene plasmid #48138) at the *BbsI* restriction site as described (Ran et al., 2013). This allows constitutive expression of sgRNAs under the U6 promoter while *Sp*Cas9 and green fluorescence protein (GFP) are expressed by the CBh promoter as two separate proteins due to the intervening self-cleaving T2A peptide. The recombinant plasmids (pSpCas9(BB)-2A-GFP-Npc1_gRNA1) and pSpCas9(BB)-2A-GFP-Npc1_gRNA2) were PCR-screened using U6 promoter sequence and respective gRNA1 or gRNA2 sequence as a reverse primer. Additionally, they were sequence

verified using a U6 promoter primer (U6 promoter sequence: 5'-ATTTCTTGGGTAGTTTGCAG- 3').

Transfection, selection, and validation of *Npc1* mutant lines

iBMDMs were transfected with 500 ng of pSpCas9(BB)-2A-GFP-Npc1_gRNA1 and pSpCas9(BB)-2A-GFP-Npc1_gRNA2 separately using 1.5 µl transfection reagent (Clontech) in 600 µl Opti-Mem media (Invitrogen) at 37 °C. After 6 h, the Opti-Mem transfection mixtures were replaced with DMEM growth media supplemented with 10% FBS and 2% penicillin/streptomycin. Cells were incubated at 37 °C in 5% CO_2 for 48 h. The transfected cells were analysed for expression of GFP (proxy for Cas9 expression) using a fluorescent microscope.

Flow cytometry-based analysis and cell sorting were performed using the BD FACS Aria II (BD Biosciences) to select Cas9 expressing cells. Forty-eight hours post transfection, the cells were trypsinized, harvested and resuspended in Sorting Buffer (SB - PBS supplemented with 2 mM EDTA and 0.1% BSA). Cells expressing Cas9 (GFP positive) were isolated by FACS (single-cell sorting) and expanded in 96-well plate.

~ 2 weeks after transfection, genomic DNA of hybridoma cell lines was prepared from typically 10^6 cells by using GenElute™ Mammalian Genomic DNA Miniprep Kit (Sigma-Aldrich, G1N70). PCR amplification was performed with primers flanking the sgRNA targeted region (Forward 5'- CTTCCTGCCTTGCGCACAC-3' and Reverse 5'-CTGTCCCTGGCTAACTGTGG-3') with the following cycling conditions: initial denaturation 5 min at 95 °C; 35 cycles with denaturation at 95 °C (30 s), annealing at 60 °C (45 s), elongation at 68 °C (45 s); final elongation at 68 °C for 5 min. An aliquot (1/10) of the PCR product was analysed by agarose gel electrophoresis; the samples were purified using Monarch® PCR & DNA Cleanup Kit (NEB, #T1030) and sequenced (Fig. S2). Out of 40 clonal cell lines screened, we found two clonal cell lines that showed deletion in the sgRNA-targeted region in the *Npc1* gene. These two independent cell lines with different deletion mutations

(KO#1 and KO#2) were expanded and used for functional analysis and used as *Npc1*-deficient (*Npc1*$^{-/-}$) cells. Since both clonal cell lines gave identical results in inflammasome activation assays (Fig. 2), henceforth, we carried out further studies using only *Npc1*$^{-/-}$ #1 cells.

Filipin Staining

Cells seeded at a density of 4 x 10^5 cells per well were grown on glass coverslips in a 24-well plate and incubated with U16888A for overnight (iBMDMs) or 48h (BMDMs) to allow cholesterol accumulation. After desired treatments, cells were fixed in 4% paraformaldehyde for 1 hour at room temperature. Cells were then stained with 25 µg/ml filipin (F9765, Sigma) overnight and washed 3 times with PBS before mounting on glass slides. Images were visualised on a Leica SP5 confocal microscope using 405 nm excitation and processed using ImageJ programme.

Cholesterol Supplementation Assay

Methyl-β-Cyclodextrin (MCD, Sigma #C4555) and cholesterol (Sigma #C8667) complexes were prepared by diluting a 25 mg/ml stock solution of cholesterol 1000-fold in serum-free DMEM containing 50 µM MCD and incubating at 50 °C in a water bath for 2 hours. Cells were plated into 12-well plates in the presence or absence of U18666a. On the day of experiment, media was replaced with serum-free DMEM and cells were primed with LPS (500 ng/ml) for 3 hours before replacing with 37 °C pre-warmed media containing cholesterol/MCD complexes. Cells were then incubated for the indicated times before addition of 5 mM ATP for 45 minutes.

Exposure to statins

BMDMs were seeded into 24- or 12-well plates and incubated overnight in media containing 5% lipid-depleted serum (S181L, Biowest). The following morning, cells were stimulated with LPS (500 ng/ml) for 3 hours before addition of fatostatin (20 µM, Tocris #4444), lovastatin (20 µM, Tocris #1530) or mevastatin (40 µM, Tocris #1526) for 1 hour. For cholesterol restoration, media was replaced following statin treatment and cells were recovered for 2 hours before addition of cholesterol for 1 hour. ATP (5 mM) was then added for 45 minutes.

Immunoblotting and antibodies

For immunoblotting of caspase-1, NLRP3, ASC, IL-1β, GSDMD, and GAPDH, cells were harvested at indicated time-points in cell lysis buffer containing NP-40, DTT, and protease inhibitors (Roche). The samples were boiled at 95°C before resolving them on 12% SDS-PAGE gels. For phospho-specific immunoblotting, cells were exposed to 500 ng/ml LPS for different time-points ranging from 30 min to 4h. Cell lysates were extracted in RIPA lysis buffer containing both protease and phosphatase inhibitors (Roche). Samples were placed on ice for 30 minutes before being centrifuged at 15000 xg for 15 minutes at 4°C to remove nuclei. The supernatant was then collected and a 10 µl aliquot was used to measure protein concentration using Pierce^{Tm} BCA Protein Assay Kit (Thermo Scientific #23227) according to the manufacturer's instructions. The protein concentration of each sample was then normalized to 1 µg/ml with RIPA lysis buffer. Equal concentration of protein samples was resolved on 6-15% SDS-PAGE gels and then transferred to nitrocellulose membranes (GE Life Sciences). Membranes were blocked for 1 hour with 5% milk solution in TBS containing 0.05% Tween-20. Membranes were incubated in primary antibodies at 4 °C overnight at the dilutions given below. HRP-conjugated secondary antibodies were used at room temperature for 1 hour. Proteins were visualised using the BioRad Clarity ECL substrate (BioRad #1705060) or the Pierce ECL Western Blotting Substrate (Thermo Scientific #32209). Images were taken on a Bio-Rad imager and processed using the manufacturer's software, Image Lab. The primary antibodies used were as follows: Caspase-1 (1:2000, AdipoGen #AG-20B-0042-C100), NLRP3 (1:2000, AdipoGen #AG-20B-0014-C100), ASC (1:2000, Adipogen #AG-25B-0006, AL177), GSDMD (1:1000, Abcam #ab209845), IL-1β (1:500, Cell Signalling #12426), AKT (1:1000, Cell Signalling #4691), phospho-AKT (1:1000, Cell Signalling #4060), p70-S6K1 (1:1000, Cell Signalling #2708), phospho–p70-S6K1 (1:1000, Cell Signalling #9234), phospho-AMPK (1:1000, Cell Signalling #2535), GAPDH (1:2500, ThermoFisher # MA5-15738). Secondary antibodies were obtained from ThermoFisher Scientific and used at a dilution of 1:5000.

Total and esterified cholesterol measurement

WT and *Npc1*$^{-/-}$ iBMDMs or primary mouse BMDMs were seeded into 12-well plates at a density of 1x10^6 per well. The following morning, the media was changed to LPDS media and cells were stimulated with LPS (500 ng/ml) for 4 hours. MCD samples were treated with 10 mM MCD for 30 min. Samples were then lysed in 140 μl of water for 30 minutes at 37 °C before being used for cholesterol measurement. Total cholesterol was measured using cholesterol Amplex Red assay kit according to manufacturer's recommendations (ThermoFisher #A12216). Unesterified cholesterol was measured by a slight modification of the original assay by omitting cholesterol esterase in the working reagent. Esterified cholesterol was calculated by subtracting the unesterfied cholesterol from the total cholesterol levels for each sample tested in triplicate. Values were normalised to protein content, which was determined using a BCA protein assay (ThermoFisher #23225)

Plasma membrane cholesterol measurement

Cholesterol concentration of the plasma membrane was measured by a cholesterol oxidase assay as previously described (Chu et al., 2015). WT and *Npc1*$^{-/-}$ iBMDMs were seeded into 24-well plates at a density of 0.5x10^6 per well. Cells were then treated with LPS and MCD as above. The cells were then washed three times with cold PBS followed by 3 washes with ice-cold assay buffer (310 mM sucrose (Sigma #S0389), 1 mM $MgSO_4$ (Sigma #M2643), 0.5 mM sodium phosphate (Na_3PO_4) [pH 7.4] (Sigma #342483). Cells were incubated with 500 µl assay buffer in the presence or absence of cholesterol oxidase (1 U/ml, Sigma #C8649) for 15 minutes at 37 °C. Next, cells were washed with PBS followed by lysis in 90 µl of water for 30 minutes at 37 °C. Total cholesterol was measured as above with Amplex Red assay for each sample tested in triplicate. Plasma membrane cholesterol was calculated by subtracting cholesterol measurements for cells exposed to cholesterol oxidase (intracellular cholesterol) from measurements obtained from cells not exposed to cholesterol oxidase (total cholesterol). Values were normalised to protein content determined as above with a BCA assay.

Quantitative Real-Time Polymerase Chain Reaction

RNA was isolated using TRIzol (Sigma # T9424) according to manufacturer's instructions. The RNA pellet was suspended in 10 µl of DNase/RNase-free water (Gibco). RNA concentration was measured in 2 µl of RNA by Nanodrop and 250 ng of total RNA was reverse transcribed into cDNA using the High capacity cDNA Reverse Transcription kit (Applied Biosystems #4368814). Real-time PCR was performed using gene specific primers and PowerUp SybrGreen (Applied Biosystems #A25741) and run on an ABI7500 or ABI7900HT (Applied Biosystems) fast real-time PCR instrument. The primers used are listed in **Table S1**.

Indirect Immunofluorescence

WT and *Npc1*$^{-/-}$ cells seeded at a density of 4 x 10^5 cells per well were grown on glass coverslips in a 24-well plate and exposed to either U16888A or statin as described above. In some samples, MitoTracker Deep Red (Invitrogen) was added in Opti-Mem media just before ATP stimulation. After desired treatments, cells were fixed in 4% paraformaldehyde for 30 min at room temperature. Cells were then labelled with the following primary antibodies for 1h at room temperature: NLRP3 (1:200, AdipoGen #AG-20B-0014-C100), Rabbit ASC (1:100, Adipogen #AG-25B-0006, AL177), Mouse ASC (1:100, Millipore #04-147, 2EI-7), calreticulin (1:200, Abcam #ab92516, EPR3924). Secondary antibodies were all obtained from Life Technologies and used according to manufacturers' recommendations. Images were visualised and acquired on a Leica SP5 confocal microscope and processed using ImageJ and Leica LAS AF programme.

ELISA

Cell culture supernatants were measured for IL-1β (eBioscience #88-7013-88), IL-18 (MBL # 7625), and TNF-α (eBioscience #88-7324-88) using ELISA kits according to the manufacturer's instructions.

Lactate Dehydrogenase Assay

Lactate dehydrogenase (LDH) was measure in the cell culture supernatant using Pierce LDH Cytotoxicity Assay Kit (ThermoFisher #88953) according to the manufacturer's instructions.

Statistical Analysis

GraphPad Prism 7.0 software was used for data analysis. Data are represented as mean ± SD or SEM and are representative of experiments done at least three times. Statistical significance was determined by unpaired Student's *t* test; $p<0.05$ was considered statistically significant.

Online Supplemental Material

Fig. S1 shows lysosomal cholesterol accumulation upon U18666a treatment and that this does not affect the priming of the NLRP3 inflammasome. Fig. S2 shows the editing of *Npc1* gene by CRISPR/Cas9. Fig. S3 shows reduction in AKT-mTOR signaling upon TLR4 ligation when NPC1 function is abrogated. Fig. S4 shows regulation of SREBP2 and plasma membrane cholesterol levels in *Npc1*$^{-/-}$ cells. Fig. S5 shows the localization of NLRP3 and ASC speck in wild-type macrophages.

Acknowledgements

We are grateful to Bao-Liang Song for discussions and suggestions at the early stage of the project. This work was supported in part by grants from The Wellcome Trust (108248/Z/15/Z), The Royal Society (RG150535) and core funds from Imperial College London to P.K.A.

The authors declare no competing financial interests.

Author Contributions

P.K.A. conceptualized the study. M.R., C.H., S.G., and P.K.A. designed methodology. M.R., C.H., R.M., and P.K.A. performed experiments. M.R., C.H., S.G., and P.K.A. analyzed data. P.K.A. wrote the original draft. P.K.A, C.H., A.A.J., and S.G. reviewed and edited the manuscript. All authors approved the final version. P.K.A provided overall supervision.

References

Altmann, S.W., H.R. Davis, L.J. Zhu, X. Yao, L.M. Hoos, G. Tetzloff, S.P.N. Iyer, M. Maguire, A. Golovko, M. Zeng, L. Wang, N. Murgolo, and M.P. Graziano. 2004. Niemann-Pick C1 Like 1 Protein Is Critical for Intestinal Cholesterol Absorption. *Science (80-.).* 303:1201–1204. doi:10.1126/science.1093131.

Amer, A., L. Franchi, T.-D. Kanneganti, M. Body-Malapel, N. Ozören, G. Brady, S. Meshinchi, R. Jagirdar, A. Gewirtz, S. Akira, and G. Núñez. 2006. Regulation of Legionella phagosome maturation and infection through flagellin and host Ipaf. *J. Biol. Chem.* 281:35217–23. doi:10.1074/jbc.M604933200.

Anand, P.K., R.K.S. Malireddi, and T.-D. Kanneganti. 2011a. Role of the Nlrp3 inflammasome in microbial infection. *Front. Microbiol.* 2. doi:10.3389/fmicb.2011.00012.

Anand, P.K., S.W.G. Tait, M. Lamkanfi, A.O. Amer, G. Nunez, G. Pagès, J. Pouysségur, M. a McGargill, D.R. Green, T.-D.D. Kanneganti, G. Pages, J. Pouyssegur, M. a McGargill, D.R. Green, and T.-D.D. Kanneganti. 2011b. TLR2 and RIP2 pathways mediate autophagy of Listeria monocytogenes via extracellular signal-regulated kinase (ERK) activation. *J. Biol. Chem.* 286:42981–42991. doi:10.1074/jbc.M111.310599.

Bauernfeind, F.G., G. Horvath, A. Stutz, E.S. Alnemri, K. MacDonald, D. Speert, T. Fernandes-Alnemri, J. Wu, B.G. Monks, K.A. Fitzgerald, V. Hornung, and E. Latz. 2009. Cutting edge: NF-kappaB activating pattern recognition and cytokine receptors license NLRP3 inflammasome activation by regulating NLRP3 expression. *J. Immunol.* 183:787–91. doi:10.4049/jimmunol.0901363.

Broz, P., J. Von Moltke, J.W. Jones, R.E. Vance, and D.M. Monack. 2010. Differential requirement for caspase-1 autoproteolysis in pathogen-induced cell death and cytokine processing. *Cell Host Microbe*. 8:471–483. doi:10.1016/j.chom.2010.11.007.

Carabeo, R.A., D.J. Mead, and T. Hackstadt. 2003. Golgi-dependent transport of cholesterol to the Chlamydia trachomatis inclusion. *Proc. Natl. Acad. Sci. U. S. A.* 100:6771–6. doi:10.1073/pnas.1131289100.

Castrillo, A., S.B. Joseph, S.A. Vaidya, M. Haberland, A.M. Fogelman, G. Cheng, and P. Tontonoz. 2003. Crosstalk between LXR and Toll-like receptor signaling mediates bacterial and viral antagonism of cholesterol metabolism. *Mol. Cell.* 12:805–816. doi:10.1016/S1097-2765(03)00384-8.

Chu, B.B., Y.C. Liao, W. Qi, C. Xie, X. Du, J. Wang, H. Yang, H.H. Miao, B.L. Li, and B.L. Song. 2015. Cholesterol transport through lysosome-peroxisome membrane contacts. *Cell*. 161:291–306. doi:10.1016/j.cell.2015.02.019.

Coppens, I., A.P. Sinai, and K.A. Joiner. 2000. Toxoplasma gondii exploits host low-density lipoprotein receptor- mediated endocytosis for cholesterol acquisition. *J. Cell Biol.*

149:167–180. doi:10.1083/jcb.149.1.167.

Cruz, J.C., S. Sugii, C. Yu, and T.Y. Chang. 2000. Role of Niemann-Pick type C1 protein in intracellular trafficking of low density lipoprotein-derived cholesterol. *J. Biol. Chem.* 275:4013–4021. doi:10.1074/jbc.275.6.4013.

Dang, E. V., J.G. McDonald, D.W. Russell, and J.G. Cyster. 2017. Oxysterol Restraint of Cholesterol Synthesis Prevents AIM2 Inflammasome Activation. *Cell*. doi:10.1016/j.cell.2017.09.029.

Ding, J., K. Wang, W. Liu, Y. She, Q. Sun, J. Shi, H. Sun, D.C. Wang, and F. Shao. 2016. Pore-forming activity and structural autoinhibition of the gasdermin family. *Nature*. 535:111–116. doi:10.1038/nature18590.

Duewell, P., H. Kono, K.J. Rayner, C.M. Sirois, G. Vladimer, F.G. Bauernfeind, G.S. Abela, L. Franchi, G. Nuñez, M. Schnurr, T. Espevik, E. Lien, K.A. Fitzgerald, K.L. Rock, K.J. Moore, S.D. Wright, V. Hornung, and E. Latz. 2010. NLRP3 inflammasomes are required for atherogenesis and activated by cholesterol crystals. *Nature*. 464:1357–1361. doi:10.1038/nature08938.

Fasano, T., P. Zanoni, C. Rabacchi, L. Pisciotta, E. Favari, M.P. Adorni, P.B. Deegan, A. Park, T. Hlaing, M.D. Feher, B. Jones, A.S. Uzak, F. Kardas, A. Dardis, A. Sechi, B. Bembi, P. Minuz, S. Bertolini, F. Bernini, and S. Calandra. 2012. Novel mutations of ABCA1 transporter in patients with Tangier disease and familial HDL deficiency. *Mol. Genet. Metab.* 107:534–541. doi:10.1016/j.ymgme.2012.08.005.

Fessler, M.B. 2016. The Intracellular Cholesterol Landscape: Dynamic Integrator of the Immune Response. *Trends Immunol.* 37:819–830. doi:10.1016/j.it.2016.09.001.

Freigang, S., F. Ampenberger, G. Spohn, S. Heer, A.T. Shamshiev, J. Kisielow, M. Hersberger, M. Yamamoto, M.F. Bachmann, and M. Kopf. 2011. Nrf2 is essential for cholesterol crystal-induced inflammasome activation and exacerbation of atherosclerosis. *Eur. J. Immunol.* 41:2040–2051. doi:10.1002/eji.201041316.

Gurung, P., J.R. Lukens, and T.-D. Kanneganti. 2015. Mitochondria: diversity in the regulation of the NLRP3 inflammasome. *Trends Mol. Med.* 21:193–201. doi:10.1016/j.molmed.2014.11.008.

Hamilton, C., L. Tan, T. Miethke, and P.K.P.K. Anand. 2017. Immunity to uropathogens: the emerging roles of inflammasomes. *Nat. Rev. Urol.* 14. doi:10.1038/nrurol.2017.25.

Hornung, V., F. Bauernfeind, A. Halle, E.O. Samstad, H. Kono, K.L. Rock, K.A. Fitzgerald, and E. Latz. 2008. Silica crystals and aluminum salts activate the NALP3 inflammasome through phagosomal destabilization. *Nat. Immunol.* 9:847–856. doi:ni.1631 [pii]\r10.1038/ni.1631 [doi].

Hornung, V., and E. Latz. 2010. Critical functions of priming and lysosomal damage for NLRP3 activation. *Eur. J. Immunol.* 40:620–623. doi:10.1002/eji.200940185.

Horton, J.D., J.L. Goldstein, and M.S. Brown. 2002. SREBPs: activators of the complete program of cholesterol and fatty acid synthesis in the liver. *J. Clin. Invest.* 109:1125–31. doi:10.1172/JCI15593.

Huynh, K.K., E. Gershenzon, and S. Grinstein. 2008. Cholesterol accumulation by macrophages impairs phagosome maturation. *J. Biol. Chem.* 283:35745–35755. doi:10.1074/jbc.M806232200.

Ikonen, E. 2008. Cellular cholesterol trafficking and compartmentalization. *Nat. Rev. Mol. Cell Biol.* 9:125–138. doi:10.1038/nrm2336.

Ilnytska, O., M. Santiana, N.Y. Hsu, W.L. Du, Y.H. Chen, E.G. Viktorova, G. Belov, A.

Brinker, J. Storch, C. Moore, J.L. Dixon, and N. Altan-Bonnet. 2013. Enteroviruses harness the cellular endocytic machinery to remodel the host cell cholesterol landscape for effective viral replication. *Cell Host Microbe*. 14:281–293. doi:10.1016/j.chom.2013.08.002.

Im, S.-S., L. Yousef, C. Blaschitz, J.Z. Liu, R.A. Edwards, S.G. Young, M. Raffatellu, and T.F. Osborne. 2011. Linking Lipid Metabolism to the Innate Immune Response in Macrophages through Sterol Regulatory Element Binding Protein-1a. *Cell Metab.* 13:540–549. doi:10.1016/j.cmet.2011.04.001.

Iyer, S., Q. He, J. Janczy, E. Elliott, Z. Zhong, A. Olivier, J. Sadler, V. Knepper-Adrian, R. Han, L. Qiao, S. Eisenbarth, W. Nauseef, S. Cassel, and F. Sutterwala. 2013. Mitochondrial cardiolipin is required for Nlrp3 inflammasome activation. *Immunity*. 39:311–323. doi:10.1016/j.immuni.2013.08.001.

Jin, T., A. Perry, J. Jiang, P. Smith, J.A. Curry, L. Unterholzner, Z. Jiang, G. Horvath, V.A. Rathinam, R.W. Johnstone, V. Hornung, E. Latz, A.G. Bowie, K.A. Fitzgerald, and T.S. Xiao. 2012. Structures of the HIN Domain: DNA Complexes Reveal Ligand Binding and Activation Mechanisms of the AIM2 Inflammasome and IFI16 Receptor. *Immunity*. 36:561–571. doi:10.1016/j.immuni.2012.02.014.

Kaul, D., P.K. Anand, and I. Verma. 2004. Cholesterol-sensor initiates M. tuberculosis entry into human macrophages. *Mol. Cell. Biochem.* 258. doi:10.1023/B:MCBI.0000012851.42642.be.

Kayagaki, N., I.B. Stowe, B.L. Lee, K. O'Rourke, K. Anderson, S. Warming, T. Cuellar, B. Haley, M. Roose-Girma, Q.T. Phung, P.S. Liu, J.R. Lill, H. Li, J. Wu, S. Kummerfeld, J. Zhang, W.P. Lee, S.J. Snipas, G.S. Salvesen, L.X. Morris, L. Fitzgerald, Y. Zhang, E.M. Bertram, C.C. Goodnow, and V.M. Dixit. 2015. Caspase-11 cleaves gasdermin D for non-canonical inflammasome signalling. *Nature*. 526:666–671. doi:10.1038/nature15541.

Kofoed, E.M., and R.E. Vance. 2011. Innate immune recognition of bacterial ligands by NAIPs determines inflammasome specificity. *Nature*. 477:592–5. doi:10.1038/nature10394.

Lauer, S., J. VanWye, T. Harrison, H. McManus, B.U. Samuel, N.L. Hiller, N. Mohandas, and K. Haldar. 2000. Vacuolar uptake of host components, and a role for cholesterol and sphingomyelin in malarial infection. *EMBO J.* 19:3556–64. doi:10.1093/emboj/19.14.3556.

Lu, F., Q. Liang, L. Abi-Mosleh, A. Das, J.K. De Brabander, J.L. Goldstein, and M.S. Brown. 2015. Identification of NPC1 as the target of U18666A, an inhibitor of lysosomal cholesterol export and Ebola infection. *Elife*. 4. doi:10.7554/eLife.12177.

Lupfer, C., P.G. Thomas, P.K. Anand, P. Vogel, S. Milasta, J. Martinez, G. Huang, M. Green, M. Kundu, H. Chi, R.J. Xavier, D.R. Green, M. Lamkanfi, C. a Dinarello, P.C. Doherty, and T.-D. Kanneganti. 2013. Receptor interacting protein kinase 2-mediated mitophagy regulates inflammasome activation during virus infection. *Nat. Immunol.* 14:480–8. doi:10.1038/ni.2563.

Lupfer, C.R., P.K. Anand, Z. Liu, K.L. Stokes, P. Vogel, M. Lamkanfi, and T.D. Kanneganti. 2014. Reactive Oxygen Species Regulate Caspase-11 Expression and Activation of the Non-canonical NLRP3 Inflammasome during Enteric Pathogen Infection. *PLoS Pathog.* 10. doi:10.1371/journal.ppat.1004410.

Man, S.M., and T.-D.D. Kanneganti. 2015. Regulation of inflammasome activation. 265.

Martinon, F., V. Pétrilli, A. Mayor, A. Tardivel, J. Tschopp, V. Petrilli, A. Mayor, A. Tardivel, J. Tschopp, and V. Pétrilli. 2006. Gout-associated uric acid crystals activate the NALP3

inflammasome. *Nature*. 440:237–241. doi:10.1038/nature04516.

Maxfield, F.R., and I. Tabas. 2005. Role of cholesterol and lipid organization in disease. *Nature*. 438:612–621. doi:10.1038/nature04399.

Maxfield, F.R., and D. Wüstner. 2012. Analysis of cholesterol trafficking with fluorescent probes. *Methods Cell Biol.* 108:367–93. doi:10.1016/B978-0-12-386487-1.00017-1.

Misawa, T., M. Takahama, and T. Saitoh. 2017. Mitochondria–Endoplasmic Reticulum Contact Sites Mediate Innate Immune Responses. Springer, Singapore. 187–197.

Nakahira, K., J.A. Haspel, V.A.K. Rathinam, S.J. Lee, T. Dolinay, H.C. Lam, J.A. Englert, M. Rabinovitch, M. Cernadas, H.P. Kim, K.A. Fitzgerald, S.W. Ryter, and A.M.K. Choi. 2011. Autophagy proteins regulate innate immune responses by inhibiting the release of mitochondrial DNA mediated by the NALP3 inflammasome. *Nat. Immunol.* doi:10.1038/ni.1980.

Pelegrin, P., and A. Surprenant. 2006. Pannexin-1 mediates large pore formation and interleukin-1β release by the ATP-gated P2X7 receptor. *EMBO J.* 25:5071–5082. doi:10.1038/sj.emboj.7601378.

Peterson, T.R., S.S. Sengupta, T.E. Harris, A.E. Carmack, S.A. Kang, E. Balderas, D.A. Guertin, K.L. Madden, A.E. Carpenter, B.N. Finck, and D.M. Sabatini. 2011. MTOR complex 1 regulates lipin 1 localization to control the srebp pathway. *Cell*. 146:408–420. doi:10.1016/j.cell.2011.06.034.

Platt, F.M., B. Boland, and A.C. van der Spoel. 2012. Lysosomal storage disorders: The cellular impact of lysosomal dysfunction. *J. Cell Biol.* 199:723–734. doi:10.1083/jcb.201208152.

Porstmann, T., C.R. Santos, B. Griffiths, M. Cully, M. Wu, S. Leevers, J.R. Griffiths, Y.L. Chung, and A. Schulze. 2008. SREBP Activity Is Regulated by mTORC1 and Contributes to Akt-Dependent Cell Growth. *Cell Metab.* 8:224–236. doi:10.1016/j.cmet.2008.07.007.

Progatzky, F., N.J. Sangha, N. Yoshida, M. McBrien, J. Cheung, A. Shia, J. Scott, J.R. Marchesi, J.R. Lamb, L. Bugeon, and M.J. Dallman. 2014. Dietary cholesterol directly induces acute inflammasome-dependent intestinal inflammation. *Nat. Commun.* 5:5864. doi:10.1038/ncomms6864.

Rajamäki, K., J. Lappalainen, K. Öörni, E. Välimäki, S. Matikainen, P.T. Kovanen, and K.K. Eklund. 2010. Cholesterol Crystals Activate the NLRP3 Inflammasome in Human Macrophages: A Novel Link between Cholesterol Metabolism and Inflammation. *PLoS One*. 5:e11765. doi:10.1371/journal.pone.0011765.

Ran, F.A., P.D. Hsu, J. Wright, V. Agarwala, D.A. Scott, and F. Zhang. 2013. Genome engineering using the CRISPR-Cas9 system. *Nat Protoc*. 8:2281–2308. doi:10.1038/nprot.2013.143.

Reboldi, A., E. V. Dang, J.G. McDonald, G. Liang, D.W. Russell, and J.G. Cyster. 2014a. 25-Hydroxycholesterol suppresses interleukin-1-driven inflammation downstream of type I interferon. *Science (80-.).* 345:679–684. doi:10.1126/science.1254790.

Reboldi, A., E. V. Dang, J.G. McDonald, G. Liang, D.W. Russell, and J.G. Cyster. 2014b. 25-Hydroxycholesterol suppresses interleukin-1-driven inflammation downstream of type I interferon. *Science (80-.).* 345:679–684. doi:10.1126/science.1254790.

Repa, J.J., G. Liang, J. Ou, Y. Bashmakov, J.M.A. Lobaccaro, I. Shimomura, B. Shan, M.S. Brown, J.L. Goldstein, and D.J. Mangelsdorf. 2000. Regulation of mouse sterol regulatory element-binding protein-1c gene (SREBP-1c) by oxysterol receptors, LXRα and LXRβ. *Genes Dev.* 14:2819–2830. doi:10.1101/gad.844900.

Ridsdale, A., M. Denis, P.-Y. Gougeon, J.K. Ngsee, J.F. Presley, and X. Zha. 2006. Cholesterol Is Required for Efficient Endoplasmic Reticulum-to-Golgi Transport of Secretory Membrane Proteins. *Mol. Biol. Cell*. 17:1593–1605. doi:10.1091/mbc.E05-02-0100.

Sarkar, S., B. Carroll, Y. Buganim, D. Maetzel, A.M. Ng, J.P. Cassady, M.A. Cohen, S. Chakraborty, H. Wang, E. Spooner, H. Ploegh, J. Gsponer, V. Korolchuk, and R. Jaenisch. 2013. Impaired autophagy in the lipid-storage disorder niemann-pick type c1 disease. *Cell Rep.* 5:1302–1315. doi:10.1016/j.celrep.2013.10.042.

Sato, R., J. Inoue, Y. Kawabe, T. Kodama, T. Takano, and M. Maeda. 1996. Sterol-dependent transcriptional regulation of sterol regulatory element-binding protein-2. *J. Biol. Chem.* 271:26461–4.

Schwerd, T., S. Pandey, H.-T. Yang, K. Bagola, E. Jameson, J. Jung, R.H. Lachmann, N. Shah, S.Y. Patel, C. Booth, H. Runz, G. Düker, R. Bettels, M. Rohrbach, S. Kugathasan, H. Chapel, S. Keshav, A. Elkadri, N. Platt, A.M. Muise, S. Koletzko, R.J. Xavier, T. Marquardt, F. Powrie, J.E. Wraith, M. Gyrd-Hansen, F.M. Platt, and H.H. Uhlig. 2016. Impaired antibacterial autophagy links granulomatous intestinal inflammation in Niemann–Pick disease type C1 and XIAP deficiency with NOD2 variants in Crohn's disease. *Gut*. gutjnl-2015-310382. doi:10.1136/gutjnl-2015-310382.

Sheedy, F.J., A. Grebe, K.J. Rayner, P. Kalantari, B. Ramkhelawon, S.B. Carpenter, C.E. Becker, H.N. Ediriweera, A.E. Mullick, D.T. Golenbock, L.M. Stuart, E. Latz, K.A. Fitzgerald, and K.J. Moore. 2013. CD36 coordinates NLRP3 inflammasome activation by facilitating intracellular nucleation of soluble ligands into particulate ligands in sterile inflammation. *Nat. Immunol.* 14:812–20. doi:10.1038/ni.2639.

Shi, J., Y. Zhao, K. Wang, X. Shi, Y. Wang, H. Huang, Y. Zhuang, T. Cai, F. Wang, and F. Shao. 2015. Cleavage of GSDMD by inflammatory caspases determines pyroptotic cell death. *Nature*. 526:660–665. doi:10.1038/nature15514.

Simons, K., and R. Ehehalt. 2002. Cholesterol, lipid rafts, and disease. *J. Clin. Invest.* 110:597–603. doi:10.1172/JCI200216390.

Simons, K., and D. Toomre. 2000. Lipid rafts and signal transduction. *Nat. Rev. Mol. Cell Biol.* 1:31–39. doi:10.1038/35036052.

Strauss, K., C. Goebel, H. Runz, W. Möbius, S. Weiss, I. Feussner, M. Simons, and A. Schneider. 2010. Exosome secretion ameliorates lysosomal storage of cholesterol in Niemann-Pick type C disease. *J. Biol. Chem.* 285:26279–88. doi:10.1074/jbc.M110.134775.

Sugii, S., P.C. Reid, N. Ohgami, H. Du, and T.Y. Chang. 2003. Distinct endosomal compartments in early trafficking of low density lipoprotein-derived cholesterol. *J. Biol. Chem.* 278:27180–27189. doi:10.1074/jbc.M300542200.

Toulmay, A., and W.A. Prinz. 2011. Lipid transfer and signaling at organelle contact sites: the tip of the iceberg. *Curr. Opin. Cell Biol.* 23:458–63. doi:10.1016/j.ceb.2011.04.006.

Vainio, S., I. Bykov, M. Hermansson, E. Jokitalo, P. Somerharju, and E. Ikonen. 2005. Defective insulin receptor activation and altered lipid rafts in Niemann-Pick type C disease hepatocytes. *Biochem. J.* 391:465–472.

Wang, Y., C. Yang, K. Mao, S. Chen, G. Meng, and B. Sun. 2013. Cellular localization of NLRP3 inflammasome. *Protein Cell*. doi:10.1007/s13238-013-2113-2.

Wojtanik, K.M., and L. Liscum. 2003. The transport of low density lipoprotein-derived cholesterol to the plasma membrane is defective in NPC1 cells. *J. Biol. Chem.* 278:14850–14856. doi:10.1074/jbc.M300488200.

Xu, J., Y. Dang, Y.R. Ren, and J.O. Liu. 2010. Cholesterol trafficking is required for mTOR activation in endothelial cells. *Proc. Natl. Acad. Sci.* 107:4764–4769. doi:10.1073/pnas.0910872107.

York, A.G., K.J. Williams, J.P. Argus, Q.D. Zhou, G. Brar, L. Vergnes, E.E. Gray, A. Zhen, N.C. Wu, D.H. Yamada, C.R. Cunningham, E.J. Tarling, M.Q. Wilks, D. Casero, D.H. Gray, A.K. Yu, E.S. Wang, D.G. Brooks, R. Sun, S.G. Kitchen, T.T. Wu, K. Reue, D.B. Stetson, and S.J. Bensinger. 2015. Limiting Cholesterol Biosynthetic Flux Spontaneously Engages Type i IFN Signaling. *Cell*. 163:1716–1729. doi:10.1016/j.cell.2015.11.045.

Yvan-Charvet, L., M. Ranalletta, N. Wang, S. Han, N. Terasaka, R. Li, C. Welch, and A.R. Tall. 2007. Combined deficiency of ABCA1 and ABCG1 promotes foam cell accumulation and accelerates atherosclerosis in mice. *J. Clin. Invest.* 117:3900–3908. doi:10.1172/JCI33372.

Zhang, Z., G. Meszaros, W.-T. He, Y. Xu, H.F. Magliarelli, L. Mailly, M. Mihlan, Y. Liu, M.P. Gámez, A. Goginashvili, A. Pasquier, O. Bielska, B. Neven, P. Quartier, R. Aebersold, T.F. Baumert, P. Georgel, J. Han, and R. Ricci. 2017. Protein kinase D at the Golgi controls NLRP3 inflammasome activation. *J. Exp. Med.* 214. doi:10.1084/jem.20162040.

Zhao, Y., J. Yang, J. Shi, Y.-N. Gong, Q. Lu, H. Xu, L. Liu, and F. Shao. 2011. The NLRC4 inflammasome receptors for bacterial flagellin and type III secretion apparatus. *Nature*. 477:596–600. doi:10.1038/nature10510.

Zhou, R., A.S. Yazdi, P. Menu, and J. Tschopp. 2011. A role for mitochondria in NLRP3 inflammasome activation. *Nature*. 469:221–225. doi:10.1038/nature10156.

Zhu, X., J.Y. Lee, J.M. Timmins, J.M. Brown, E. Boudyguina, A. Mulya, A.K. Gebre, M.C. Willingham, E.M. Hiltbold, N. Mishra, N. Maeda, and J.S. Parks. 2008. Increased cellular free cholesterol in macrophage-specific Abca1 knock-out mice enhances pro-inflammatory response of macrophages. *J. Biol. Chem.* 283:22930–22941. doi:10.1074/jbc.M801408200.

Zhu, X., M.M. Westcott, X. Bi, M. Liu, K.M. Gowdy, J. Seo, Q. Cao, A.K. Gebre, M.B. Fessler, E.M. Hitbold, and J.S. Parks. 2012. Myeloid cell-specific ABCA1 deletion protects mice from bacterial infection. *Circ. Res.* 111:1398–1409. doi:10.1161/CIRCRESAHA.112.269043.

Figure Legends

Figure 1. Lysosomal sterol accumulation dampens inflammasome activation. (A) Bone marrow derived macrophages (BMDMs) were incubated with U18666a in the presence or absence of LPS followed by measurement of total cholesterol **(B**) BMDMs were either left untreated or exposed to 5 µg/ml U18666a before treating them with LPS (500 ng/ml, 4 h) and ATP (5 mM, 45 mins). Cell lysates were immunoblotted for caspase-1 antibody, and GAPDH as loading control. **(C)** IL-1β release from cells treated as above. **(D)** BMDMs were either left untreated or exposed to increasing concentrations of U18666a (1, 2, 5, 10 µg/ml) before stimulating them with LPS and ATP. Cell lysates were immunoblotted for the antibodies indicated and **(E)** cell supernatants were analysed for IL-1β, or **(F)** IL-18 by ELISA. **(G)** Microscopy images of cells treated as above in **(B),** or with Pam3 (500 ng/ml, 4 h) followed by ATP, showing characteristic pyroptotic cell death. Scale bars, 20 µm. **(H, I)** LDH release in supernatants from cells treated as in **(G)**. **(J, K)** LPS-primed BMDMs treated with indicated concentrations of bafilomycin A1 (BafA1) **(J)** or chloroquine (CQ) **(K)** followed by ATP. Data shown are mean ± SD, and experiments shown are representative of at least three independent experiments. **, $p < 0.01$; ***, $p < 0.001$; ****, $p < 0.0001$, by Student's *t* test.

Figure 2. Deficiency in *Npc1* abrogates NLRP3 inflammasome activation. (A) Confocal microscopy images of wild-type and *Npc1*$^{-/-}$ iBMDMs stained with filipin. Note that two different clonal cells lines of *Npc1*$^{-/-}$ (#1, #2) are shown. Scale bars, 10 µm **(B)** WT and *Npc1*$^{-/-}$ cells were either left untreated or treated with LPS (500 ng/ml, 4 h) and nigericin (20 nM, 45 mins). Cell lysates were immunoblotted for antibodies indicated, and **(C, D, E)** cell supernatants were analysed for IL-1β, IL-18 and TNF-α by ELISA. **(F)** WT and *Npc1*$^{-/-}$ cells were either left untreated or treated with LPS (500 ng/ml, 4 h) and ATP (5 µM, 45 mins). Cell lysates were immunoblotted for antibodies indicated, and **(G, H)** cell supernatants were analysed for IL-1β and TNF-α by ELISA. **(I)** Microscopy images of cells treated as above in **(B)** showing characteristic pyroptotic cell death. Scale bars, 20 µm. Data shown are mean ± SD, and

experiments shown are representative of at least three independent experiments. ***, $p < 0.001$; ****, by Student's *t* test.

Figure 3. *Npc1* deficiency does not affects the activation of NLRC4 and AIM2 inflammasomes. (A) WT iBMDMs were incubated with or without the presence of increasing concentrations of U18666a (2, 5, 10 µg/ml) alongside *Nlrc4*$^{-/-}$ cells and subsequently infected with *Salmonella typhimurium* at an MOI of 2 for approximately 4 hours. Cell lysates were immunoblotted for caspase-1 and GAPDH. **(B)** WT and *Npc1*$^{-/-}$ cells were treated with *S. typhimurium* for 4 hours and immunoblotted as in **(A). (C)** Cell supernatants were analysed for IL-1β. **(D)** WT cells either treated or not with U18666a (5 µg/ml) and *Npc1*$^{-/-}$ cells were transfected with poly(dA:dT) for 4 hours before cell lysates were immunoblotted for the antibodies indicated. **(E)** WT, *Asc*$^{-/-}$ and *caspase 1/11*$^{-/-}$ cells were exposed or not to U18666a before infection with *S. typhimurium* as above. Cell lysates were immunoblotted for Gasdermin-D and GAPDH. **(F, G)** BMDMs were treated with either LPS (500 ng/ml, 4h) or Pam3 (500 ng/ml, 4h) in the presence of increasing concentrations of U18666a (1, 2, 5, 10 µg/ml) followed by ATP (5 mM, 45 mins). Cell lysates were immunoblotted for Gasdermin-D and GAPDH.

Figure 4. Cholesterol supplementation restores inflammasome activation in cells defective in NPC1 function. (A) BMDMs were either left untreated or exposed to LPS and cholesterol/MCD complexes (chol), or cholesterol and ATP, or LPS and ATP in the presence or absence of 5 µg/ml U18666a. Where added, cells were incubated with 15 µg/ml cholesterol for 1h before ATP treatment. Samples were immunoblotted with caspase-1, and GAPDH was used as a loading control. **(B)** Cell supernatants were analysed for secreted IL-1β by ELISA. Bar graph shows percent IL-1β restoration when cholesterol/MCD was added. **(C)** IL-1β levels in LPS-primed BMDMs grown in complete DMEM and exposed to alum (1 mg/ml). **(D)** IL-1β

levels in *Npc1*$^{-/-}$ cells either left untreated or treated with LPS and cholesterol/MCD for 1 h followed by ATP. **(E)** BMDMs were either left untreated or exposed to LPS and ATP in the presence or absence of 5 μg/ml U18666a. Where added, cells were incubated with indicated concentrations of cholesterol/MCD for 1h before ATP treatment. Samples were immunoblotted with the indicated antibodies. GAPDH was used as a loading control. **(F)** Cell supernatants from above were analysed for secreted IL-1β by ELISA. Bar graph shows percent IL-1β restoration when cholesterol/MCD was added. Data shown are mean ± SD, and experiments shown are representative of at least three independent experiments. **, $p < 0.01$; ***, $p < 0.001$; ****, $p < 0.0001$, by Student's *t* test.

Figure 5. Cholesterol depletion in the ER membranes abrogates caspase-1 activation and IL-1β secretion. (A) Total cholesterol levels in control or LPS treated BMDMs in the presence or absence of MCD. **(B, C)** BMDMs were treated as in **(A)** followed by the addition of ATP. Cell lysates were immunoblotted for caspase-1 **(B)** and supernatants were analysed for IL-1β **(C). (D)** WT and *Npc1*$^{-/-}$ cells were treated with LPS (500 ng/ml, 4 h) before measurement of esterified cholesterol. **(E, G)** IL-1β levels in LPS-primed BMDMs exposed to fatostatin **(E)**, or lovastatin, or mevastatin **(G)** for 1h before the addition of ATP. **(F)** Caspase-1 immunoblotting of cell lysates treated as described above and indicated. **(H)** Secreted IL-1β levels upon addition of cholesterol/MCD for 1h before ATP stimulation from BMDM treated as above in **(G). (I)** BMDMs were either treated with LPS+ATP or transfected with poly(dA:dT) (1 μg/ml, 4h) in the presence or absence of lovastatin (40 μM) during the final 1h. Cell lysates were immunoblotted for the antibodies indicated. **(J, K)** Cells were treated as in **(I)** and cell supernatants were analysed for IL-18 **(J)** and IL-1β **(K)**. Data shown are mean ± SD, and experiments shown are representative of at least three independent experiments. n.s., not significant. *, $p < 0.05$; **, $p < 0.01$; ***, $p < 0.001$; ****, $p < 0.0001$, by Student's *t* test.

Figure 6. ER cholesterol depletion blunts ASC-dependent inflammasome assembly. (A) WT (control), U18666a-treated, and *Npc1*$^{-/-}$ cells were exposed to LPS+ATP followed by labelling with anti-ASC antibody and DAPI staining. **(B)** Quantitative analysis of percentage of cells with ASC specks in samples treated as above. Each dot represents an individual field with at least n=40 cells. **(C)** LPS-primed BMDMs exposed to ATP, or **(D)** poly(dA:dT) transfected BMDMs, were exposed or not to lovastatin (40 μM, 1h) followed by labelling with anti-ASC antibody and DAPI staining. **(E)** Quantitative analysis of percentage of cells with ASC specks in samples treated as above. Each dot represents an individual field with at least n=30 cells. Data shown are mean ± SEM, and experiments shown are representative of at least three independent experiments. Scale bars, 5 μm. n.s., not significant. ****, $p < 0.0001$, by Student's *t* test.

Figure 7. NLRP3 recruitment to ASC is diminished in *Npc1*$^{-/-}$ cells. (A, C) WT and *Npc1*$^{-/-}$ cells were exposed to LPS+ATP and subsequently fixed and labelled for NLRP3 and ASC with secondary antibodies conjugated to FITC and Alexa Fluor 546, respectively. Inset shows zoom of indicated region on the middle panel. Scale bars, 10 μm. **(B, D)** Profile of fluorescence intensity along the indicated white bar in inset in A and C, respectively. Scale bars, 10 μm. **(E)** Quantitative analysis showing the percentage of cells that show NLRP3 and ASC association. At least 10 random fields were selected each with n=15 cells. Data shown are mean ± SD, and experiments shown are representative of at least three independent experiments. ****, $p < 0.0001$, by Student's *t* test. **(F, G)** Schematic model describing the identified mechanism in the activation of the NLRP3 inflammasome. **(F)** Homeostatic cellular cholesterol trafficking to the ER is required for optimal inflammasome activation. **(G)** Blockade of cholesterol transporter, NPC1, leads to lysosomal cholesterol accumulation, and a subsequent decrease in cholesterol pool in both the endoplasmic reticulum (ER) and the plasma membrane (PM). This in turn leads to decreased phosphorylation of AKT and mTOR following TLR ligation, causing a reduction in SREBP2-dependent lipogenesis. Additionally, perturbation in the ER

cholesterol levels leads to decreased association of NLRP3 and ASC resulting in reduced active caspase-1 levels and IL-1β secretion. Furthermore, inhibition of ER cholesterol levels by statins similarly blunts NLRP3 inflammasome activation.

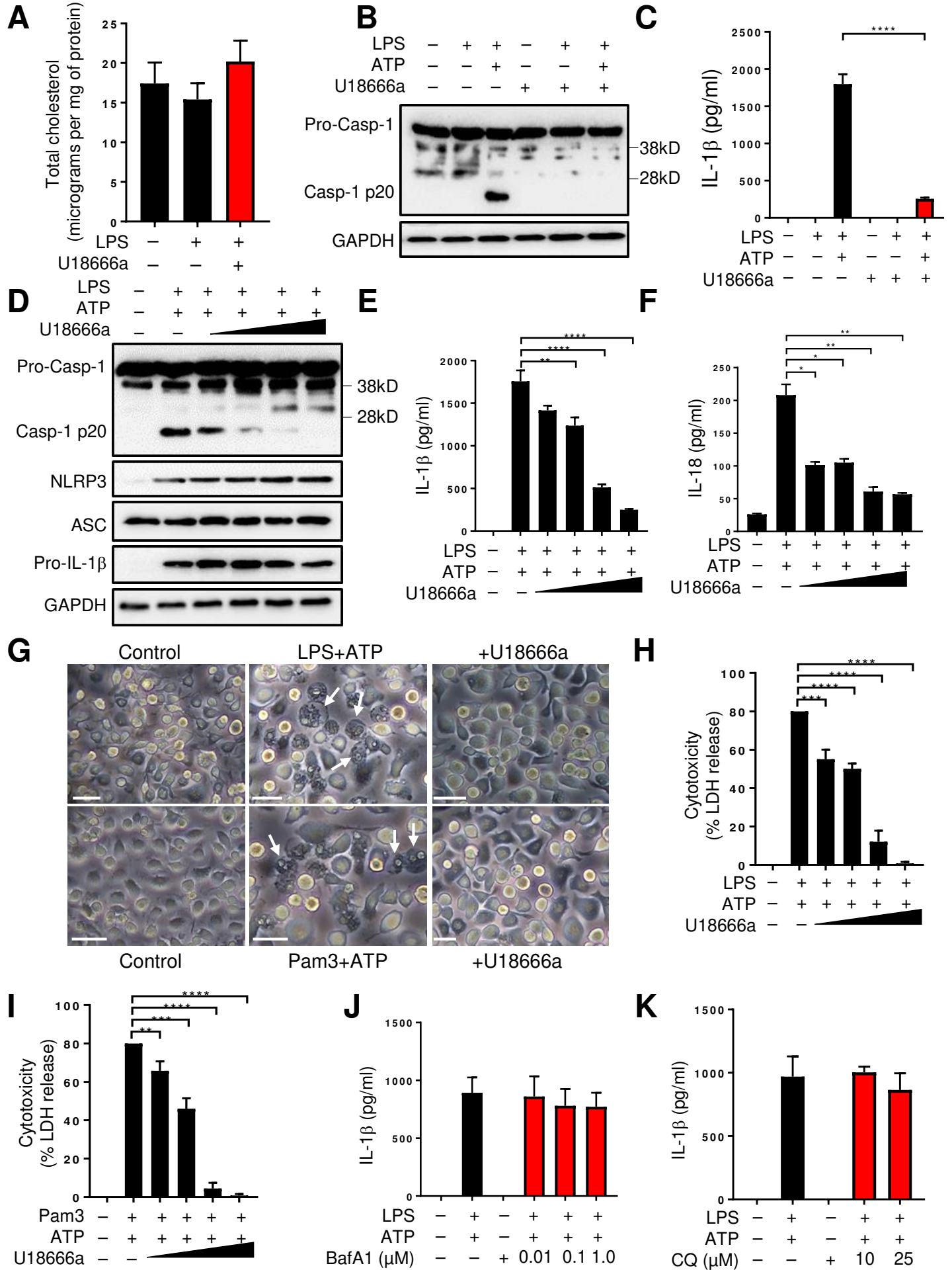
A
Total cholesterol (micrograms per mg of protein)
LPS
U18666a
B
LPS
ATP
U18666a
Pro-Casp-1
Casp-1 p20
GAPDH
38kD
28kD
C
IL-1β (pg/ml)
****
D
Pro-Casp-1
Casp-1 p20
NLRP3
ASC
Pro-IL-1β
GAPDH
38kD
28kD
E
IL-1β (pg/ml)
F
IL-18 (pg/ml)
G
Control
LPS+ATP
+U18666a
Pam3+ATP
H
Cytotoxicity (% LDH release)
I
Pam3
J
IL-1β (pg/ml)
BafA1 (μM)
0.01
0.1
1.0
K
CQ (μM)
10
25

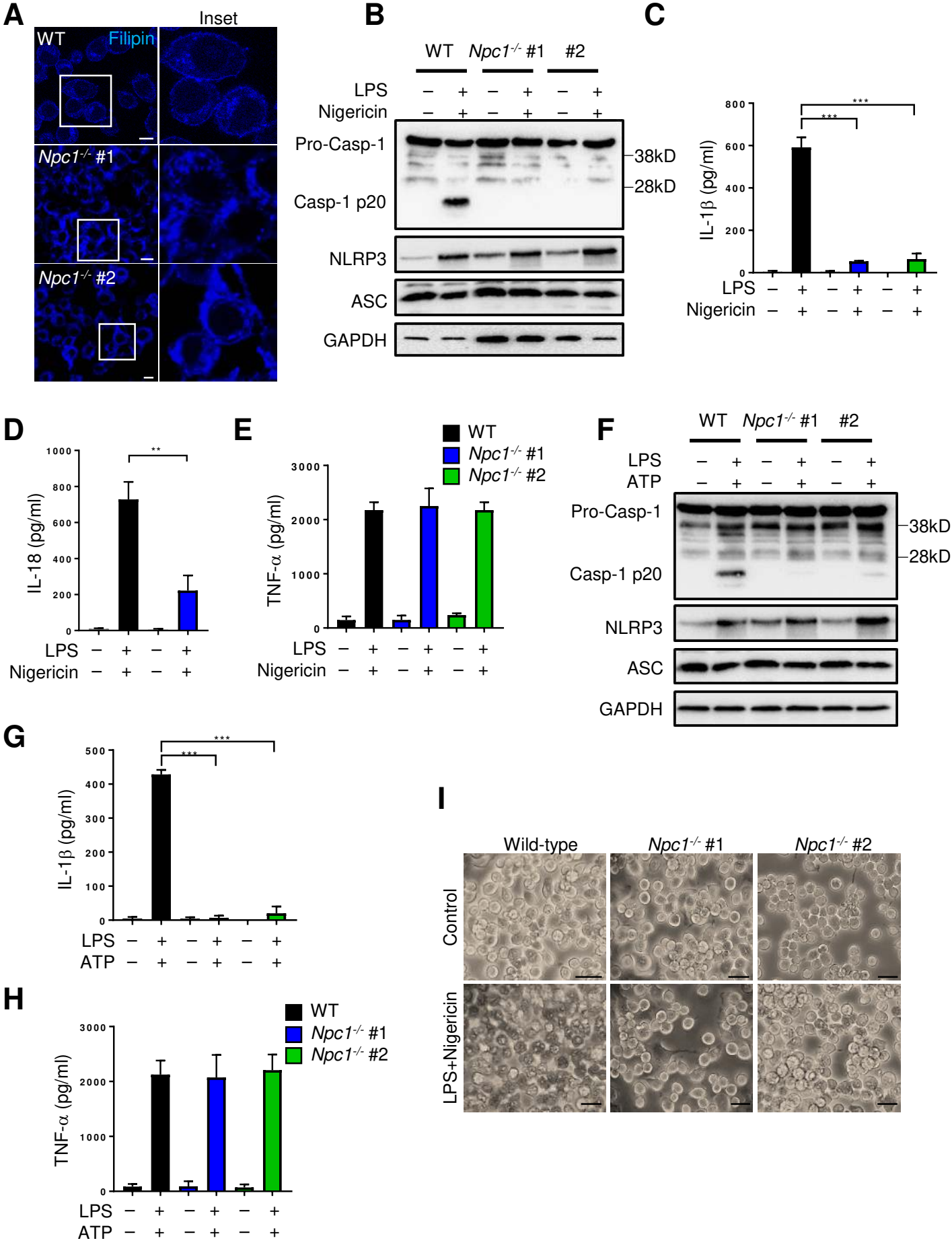
A
Inset
WT
Filipin
Npc1-/- #1
Npc1-/- #2
B
WT
Npc1-/- #1
#2
LPS
Nigericin
Pro-Casp-1
Casp-1 p20
38kD
28kD
NLRP3
ASC
GAPDH
C
IL-1β (pg/ml)
LPS
Nigericin
D
IL-18 (pg/ml)
LPS
Nigericin
E
WT
Npc1-/- #1
Npc1-/- #2
TNF-α (pg/ml)
LPS
Nigericin
F
WT
Npc1-/- #1
#2
LPS
ATP
Pro-Casp-1
Casp-1 p20
38kD
28kD
NLRP3
ASC
GAPDH
G
IL-1β (pg/ml)
LPS
ATP
H
WT
Npc1-/- #1
Npc1-/- #2
TNF-α (pg/ml)
LPS
ATP
I
Wild-type
Npc1-/- #1
Npc1-/- #2
Control
LPS+Nigericin

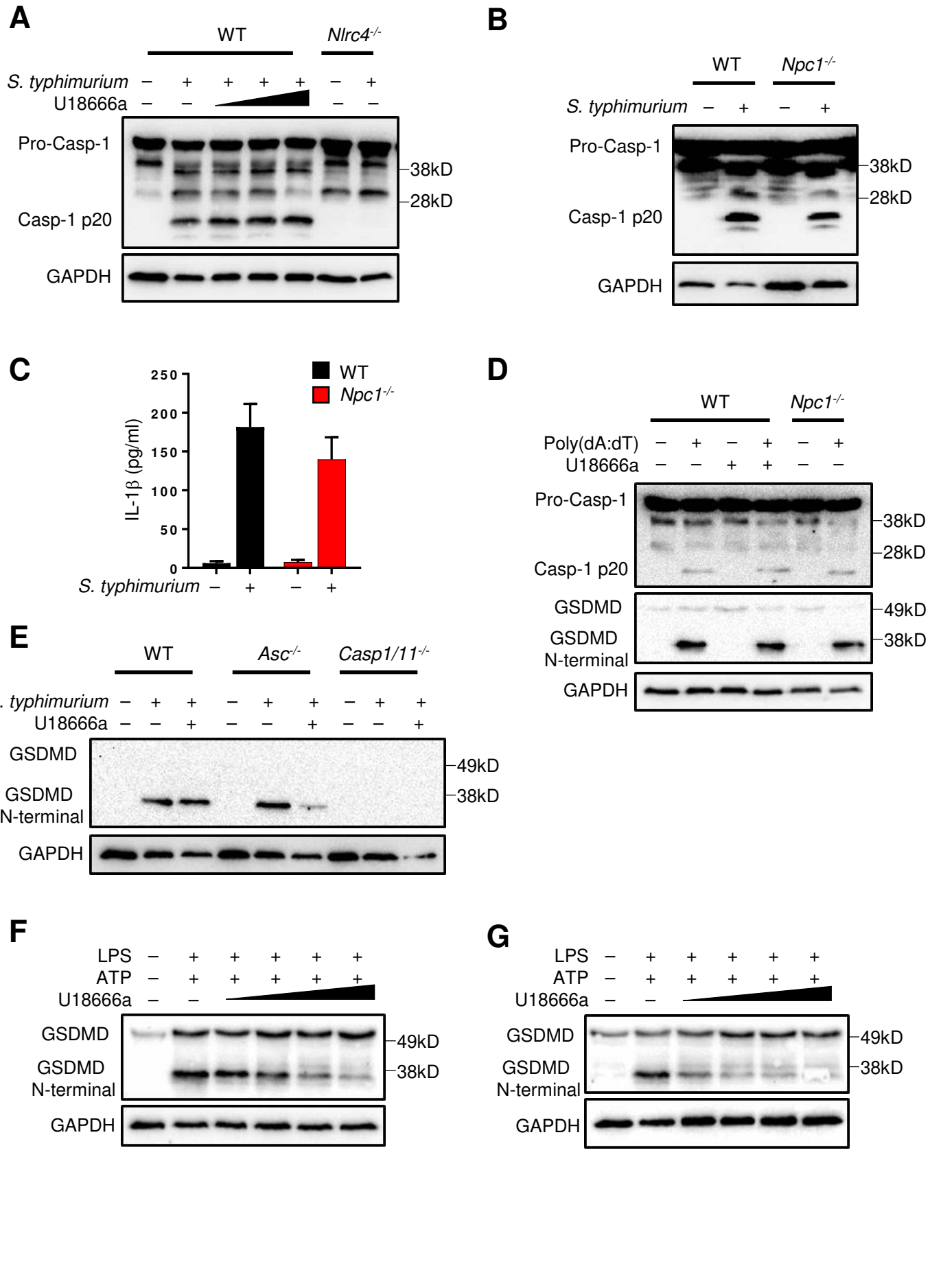
A
WT
Nlrc4-/-
S. typhimurium
U18666a
Pro-Casp-1
Casp-1 p20
GAPDH
38kD
28kD
B
WT
Npc1-/-
S. typhimurium
Pro-Casp-1
Casp-1 p20
GAPDH
38kD
28kD
C
WT
Npc1-/-
IL-1β (pg/ml)
250
200
150
100
50
0
S. typhimurium
D
WT
Npc1-/-
Poly(dA:dT)
U18666a
Pro-Casp-1
Casp-1 p20
GSDMD
GSDMD N-terminal
GAPDH
38kD
28kD
49kD
38kD
E
WT
Asc-/-
Casp1/11-/-
S. typhimurium
U18666a
GSDMD
GSDMD N-terminal
GAPDH
49kD
38kD
F
LPS
ATP
U18666a
GSDMD
GSDMD N-terminal
GAPDH
49kD
38kD
G
LPS
ATP
U18666a
GSDMD
GSDMD N-terminal
GAPDH
49kD
38kD

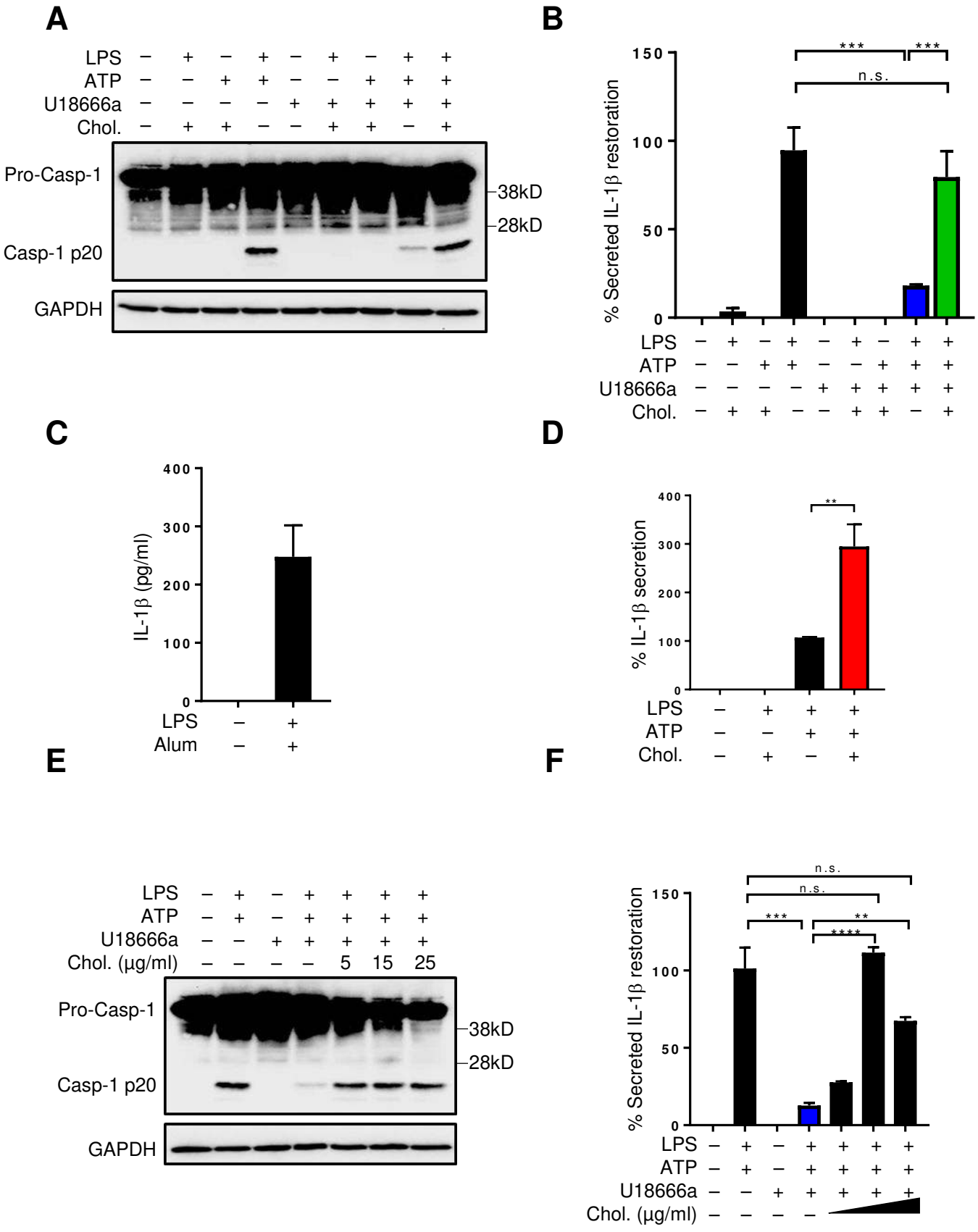
A
LPS
ATP
U18666a
Chol.
Pro-Casp-1
Casp-1 p20
GAPDH
38kD
28kD
B
% Secreted IL-1β restoration
150
100
50
0
***
***
n.s.
LPS
ATP
U18666a
Chol.
C
IL-1β (pg/ml)
400
300
200
100
0
LPS
Alum
D
% IL-1β secretion
400
300
200
100
0
**
LPS
ATP
Chol.
E
LPS
ATP
U18666a
Chol. (μg/ml)
5
15
25
Pro-Casp-1
Casp-1 p20
GAPDH
38kD
28kD
F
% Secreted IL-1β restoration
150
100
50
0
n.s.
n.s.
***
**
****
LPS
ATP
U18666a
Chol. (μg/ml)

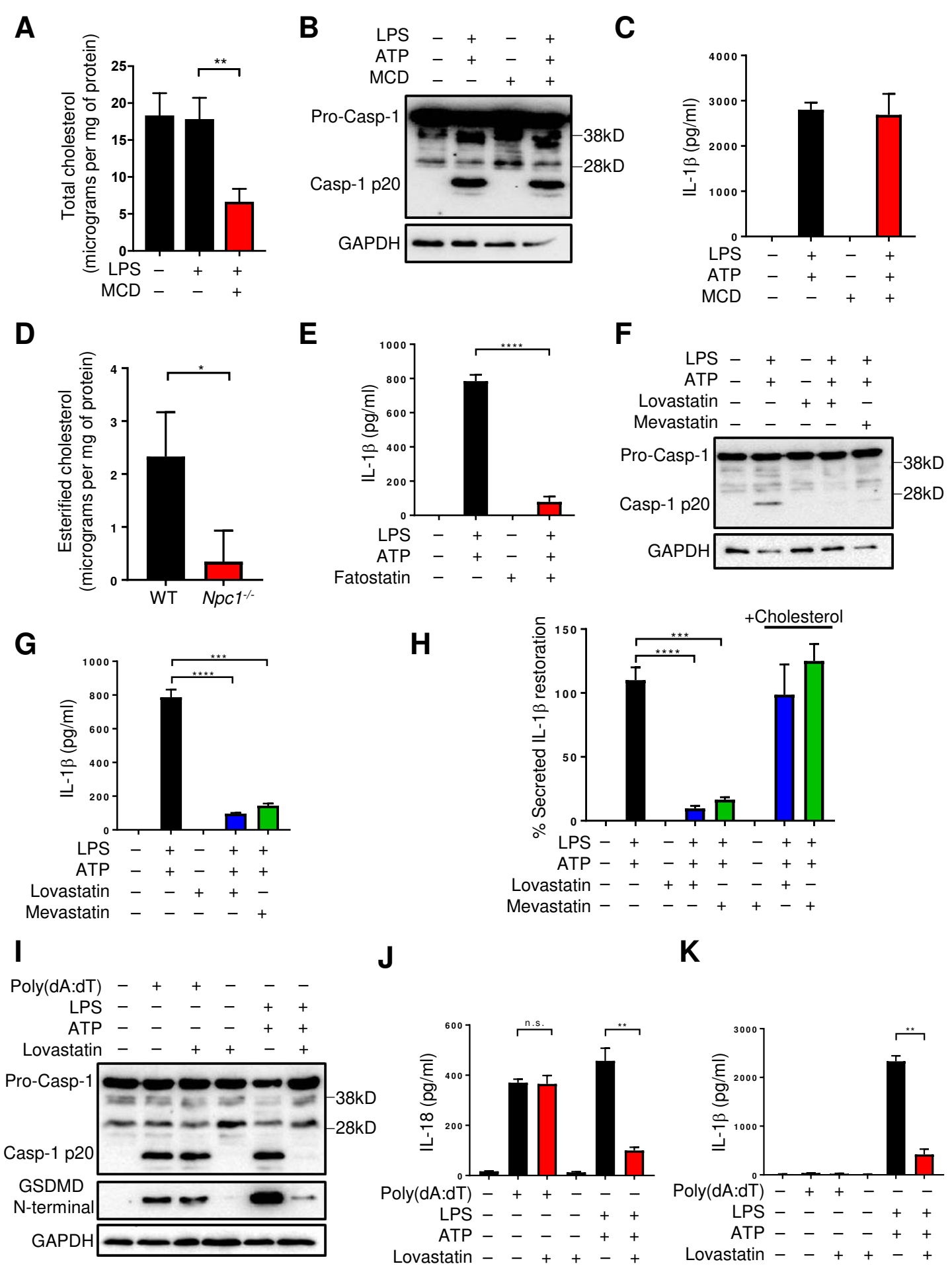
A
Total cholesterol (micrograms per mg of protein)
LPS
MCD
B
LPS
ATP
MCD
Pro-Casp-1
Casp-1 p20
GAPDH
38kD
28kD
C
IL-1β (pg/ml)
LPS
ATP
MCD
D
Esterified cholesterol (micrograms per mg of protein)
WT
Npc1-/-
E
IL-1β (pg/ml)
LPS
ATP
Fatostatin
F
LPS
ATP
Lovastatin
Mevastatin
Pro-Casp-1
Casp-1 p20
GAPDH
38kD
28kD
G
IL-1β (pg/ml)
LPS
ATP
Lovastatin
Mevastatin
H
+Cholesterol
% Secreted IL-1β restoration
LPS
ATP
Lovastatin
Mevastatin
I
Poly(dA:dT)
LPS
ATP
Lovastatin
Pro-Casp-1
Casp-1 p20
GSDMD N-terminal
GAPDH
38kD
28kD
J
IL-18 (pg/ml)
n.s.
Poly(dA:dT)
LPS
ATP
Lovastatin
K
IL-1β (pg/ml)
Poly(dA:dT)
LPS
ATP
Lovastatin

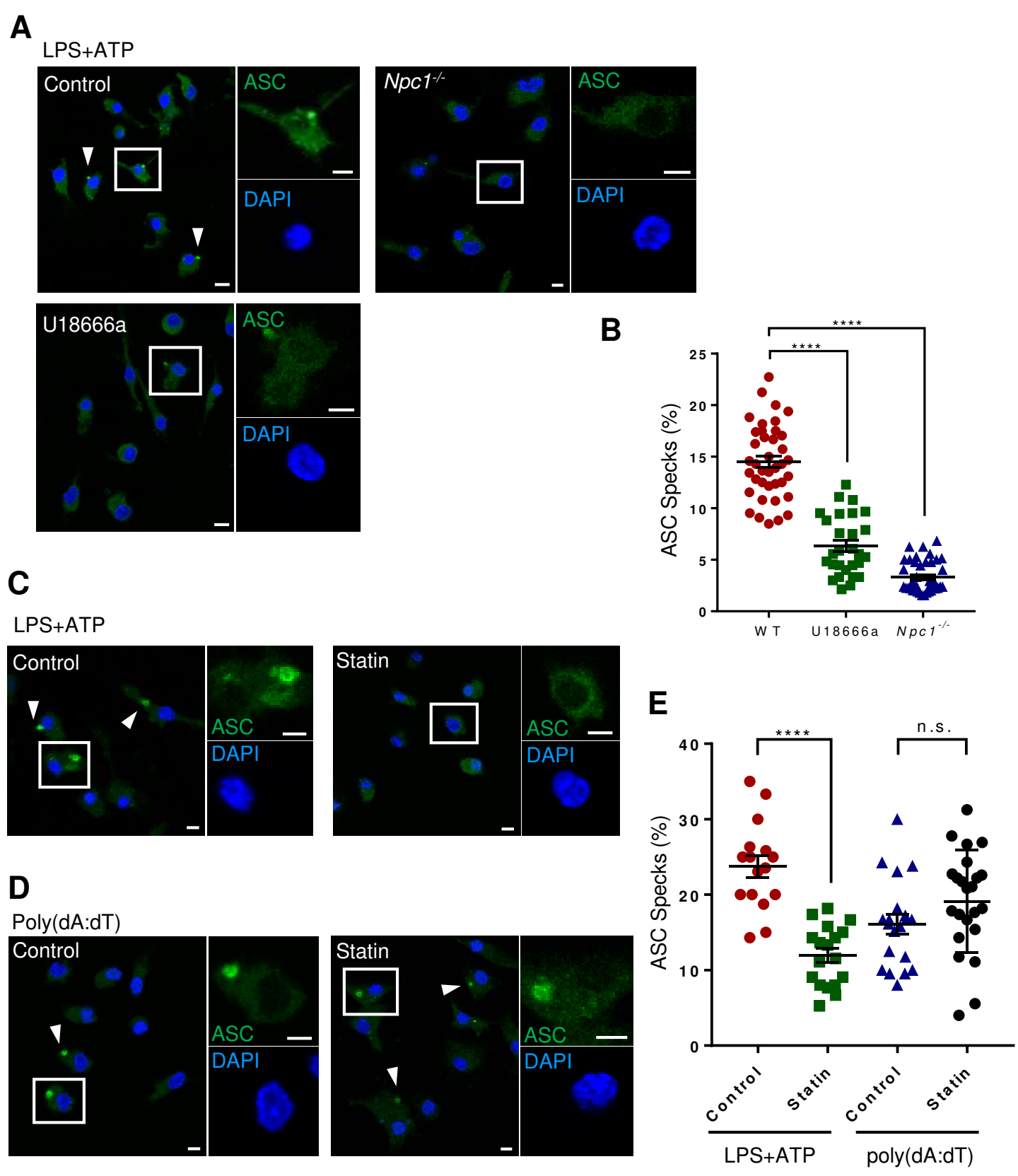
A
LPS+ATP
Control
ASC
DAPI
Npc1-/-
ASC
DAPI
U18666a
ASC
DAPI
B
ASC Specks (%)
25
20
15
10
5
0
****
****
WT
U18666a
Npc1-/-
C
LPS+ATP
Control
ASC
DAPI
Statin
ASC
DAPI
D
Poly(dA:dT)
Control
ASC
DAPI
Statin
ASC
DAPI
E
ASC Specks (%)
40
30
20
10
0
****
n.s.
Control
Statin
Control
Statin
LPS+ATP
poly(dA:dT)

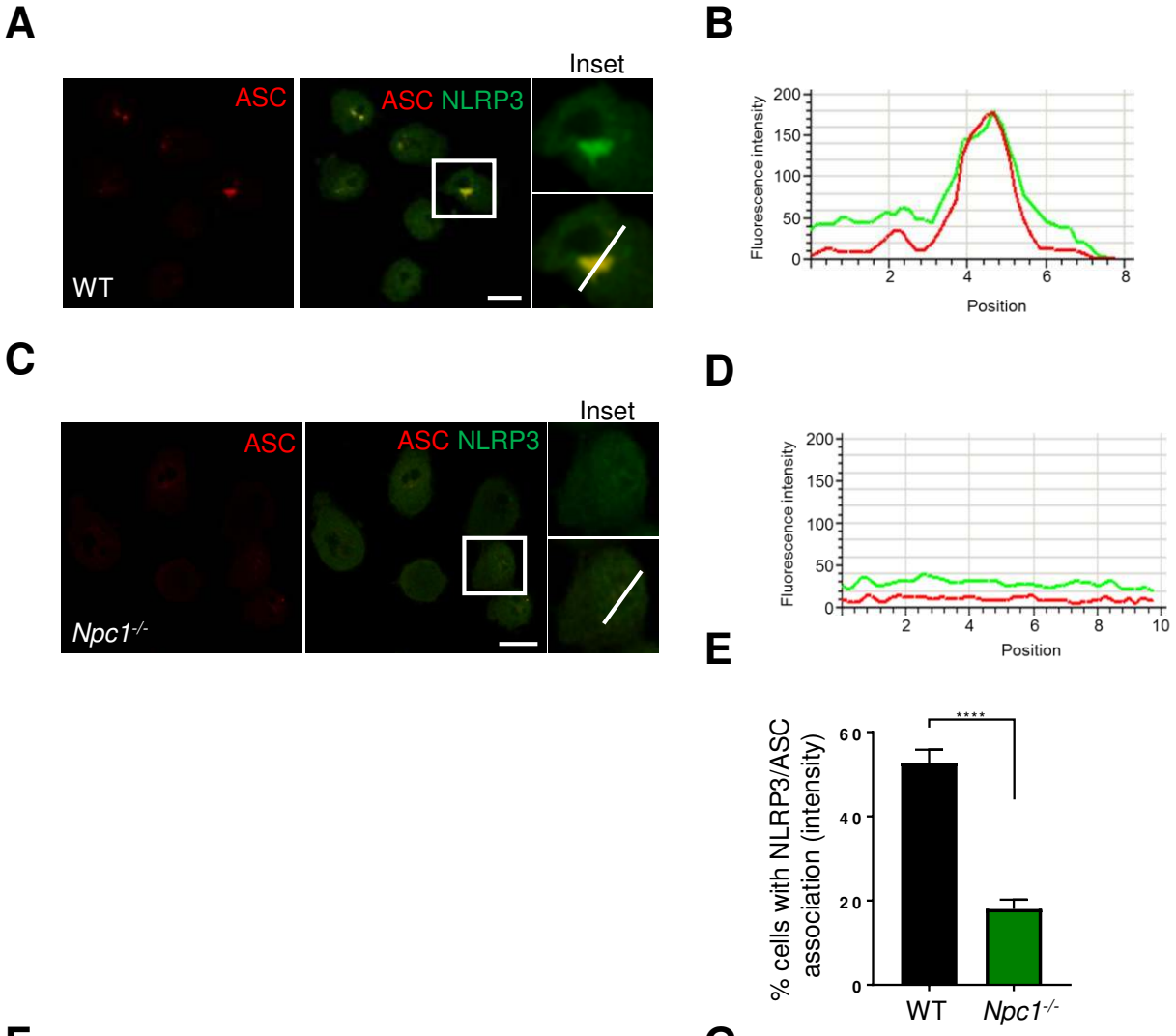
A
Inset
ASC
ASC NLRP3
WT
B
Fluorescence intensity
200
150
100
50
0
2
4
6
8
Position
C
Inset
ASC
ASC NLRP3
Npc1-/-
D
Fluorescence intensity
200
150
100
50
0
2
4
6
8
10
Position
E
****
% cells with NLRP3/ASC association (intensity)
60
40
20
0
WT
Npc1-/-
F
TLR
Cholesterol (PM)
Cholesterol (Late-lysosome)
LDL-R
pAKT
pmTOR
Cholesterol (ER)
NPC1
SREBP2
NLRP3
NLRP3
ASC
Casp-1
SREBP2
NF-κB
pro-IL-1β
IL-1β
Cholesterol (PM)
G
TLR
Reduced PM cholesterol
Cholesterol (Late-lysosome)
LDL-R
pAKT
pmTOR
Statin
Cholesterol (ER)
NPC1-deficiency
SREBP2
NLRP3
Cleaved Casp-1
SREBP2
NF-κB
pro-IL-1β

Supplementary Figure Legends

Figure S1. U18666a treatment results in lysosomal cholesterol accumulation and does not affect the priming step of the NLRP3 inflammasome.

(A) Primary BMDMs grown on coverslips were either left untreated (control) or treated with 5 μg/ml U18666a (+U) for 48 h before staining them with filipin (25 μg/ml). **(B)** iBMDMs grown on coverslips were either left untreated (control) or treated with 5 μg/ml U18666a (+U) overnight before staining them with filipin (25 μg/ml). Note the punctate structures in U18666a treated cells in **(A, B)** showing lysosomal cholesterol accumulation. Scale bars, 5 μm. **(C)** Primary BMDMs were either left untreated or exposed to increasing concentrations of itraconazole (1 μg/ml and 2 μg/ml) prior to LPS (500 ng/ml, 4 h) and ATP (5 mM, 45 mins) stimulation. Cell lysates were immunoblotted for caspase-1 and cell supernatants were analysed for IL-1β by ELISA. **(D)** Primary BMDMs were either left untreated or exposed to increasing concentrations of U18666a (1, 2, 5, 10 μg/ml) followed by Pam3 (500 ng/ml, 4 h) and ATP (5 mM, 45 mins) stimulation. Cell lysates were immunoblotted for the antibodies indicated, and **(E)** cell supernatants were analysed for IL-1β by ELISA. **(F)** Wild-type and *Nlrp3*$^{-/-}$ iBMDMs were either left untreated or exposed to increasing concentrations of U18666a (1, 2, 5 μg/ml) before stimulating them with LPS (500 ng/ml, 4 h) and nigericin (20uM, 45 mins). Cell lysates were immunoblotted for caspase-1, and GAPDH as loading control. Cell supernatants were analysed for **(G)** IL-1β and **(H)** TNF-α by ELISA. **(I)** BMDMs were either left untreated or exposed to increasing concentrations of U18666a (1, 2, 5, 10 μg/ml) followed by LPS (500 ng/ml, 4 h) and ATP (5 mM, 45 mins) stimulation. TNF-α release in cells supernatants was measured by ELISA. **(J)** BMDMs were treated as in **(D)** above and TNF-α release was measured by ELISA. **(K-M)** BMDMs were either left untreated (control) or exposed to 5 μg/ml of U18666a before stimulating cells with LPS (500 ng/ml). RNA samples were collected at different time post-LPS stimulation and expression of genes coding for *Nlrp3, Tnf, and Il-6* was evaluated by quantitative real-time PCR. Bar graphs show levels of target

genes relative to controls and are normalized to *Gapdh*. Data shown are mean ± SD, and experiments shown are representative of at least three independent experiments. *, $p < 0.05$; **, $p < 0.01$; ***, $p < 0.001$; ****, $p < 0.0001$, by Student's *t* test.

Figure S2. Editing of *Npc1* gene by CRISPR/Cas9 and reduced SREBP2 activation in *Npc1*$^{-/-}$ cells.

(A) Agarose gel showing DNA fragments generated by PCR amplification of the region targeted by sgRNAs using flanking primer pair. Each lane shows an individual clonal cell line. Note that two of the clonal cell lines indicated by asterisk show bands with a smaller amplicon size suggesting deletion and correspond to KO#1 and KO#2 cell line, respectively **(B)** Schematic diagram showing Sanger sequencing of the DNA fragment obtained in **(A)** above from wild-type (*Npc1*-WT), and two *Npc1*-deficient (*Npc1*-KO#1 and *Npc1*-KO#2) cell lines. The sequence of the targeting sgRNAs are underlined in *Npc1*-WT. The *Npc1*-KO#1 was generated using gRNA 1 (nt 49-68) while *Npc1*-KO#2 was obtained from gRNA2 (nt 81-100) containing plasmids. Deleted sequences in *Npc1*-deficient (*Npc1*-KO#1 and *Npc1*-KO#2) cell lines are shown by dashed lines. **(C)** *Npc1* transcript expression in LPS primed wild-type (*Npc1*-WT), and two *Npc1*-deficient (*Npc1*-KO#1 and *Npc1*-KO#2) cell lines. Bar graph shows levels of *Npc1* mRNA in *Npc1*-KO cell lines relative to the wild-type and are normalized to *Gapdh*. **(D-F)** Wild type and *Npc1*$^{-/-}$ were stimulated with LPS (500 ng/ml). RNA samples were collected at 4 h post-LPS stimulation and expression of genes coding for *Srebp2, Hmgcs1*, and *Hmgcr* was quantified by real-time PCR. Bar graphs show levels of target genes relative to control untreated cells (control) and are normalized to *Gapdh*. **(G-I)** BMDMs were exposed to mTOR inhibitor Torin1 (50 nM and 100 nM, 2h) before stimulating them with LPS (500 ng/ml). RNA samples were collected at 4 h post-LPS stimulation and expression of genes coding for *Srebp2, Hmgcs1*, and *Hmgcr* was quantified by real-time PCR. Bar graphs show levels of target genes relative to *Gapdh*. Data shown are mean ± SD, and experiments shown are representative of at least three independent experiments. *, $p < 0.05$; **, $p < 0.01$; ***, $p <$

0.001, by Student's *t* test.

Figure S3. Blockade of NPC1 function disengages the AKT-mTOR pathway.

(A, D) BMDMs were either left untreated or exposed to 5 µg/ml U18666a before stimulating with LPS (500 ng/ml) for the indicated times. Samples were immunoblotted with the indicated antibodies. GAPDH was used as a loading control. **(B, E)** Wild type and *Npc1*$^{-/-}$ cells were stimulated with LPS (500 ng/ml) for indicated times. Samples were immunoblotted with the indicated antibodies. GAPDH was used as a loading control. **(C, F)** Bar graphs showing semi-quantification of phosphorylated S6K1 and phosphorylated AKT levels relative to total S6K1 and total AKT levels, respectively.

Figure S4. Regulation of SREBP2 and plasma membrane cholesterol levels in *Npc1*$^{-/-}$ cells.

(A) RNA from control unstimulated wild type and *Npc1*$^{-/-}$ was collected and expression of genes coding for *Srebp2 and Hmgcs1* was quantified by real-time PCR. Bar graphs show levels of target genes normalized to *Gapdh*. **(B)** Plasma membrane cholesterol levels in WT cells either exposed or not to MCD (10 mM, 30min) and *Npc1*$^{-/-}$ cells. **(C)** WT iBMDMs grown overnight in lipid-depleted media were exposed to SREBP inhibitor fatostatin (40 µM). RNA samples were collected at indicated times and expression of genes coding for *Srebp2, Hmgcs1*, and *Hmgcr* was quantified by real-time PCR. Bar graphs show levels of target genes relative to *Gapdh*. **(D)** Secreted IL-1β levels upon addition of mevalonate for 4h before ATP stimulation from BMDM treated as in **5G.** Data shown are mean ± SD, and experiments shown are representative of at least three independent experiments. *, $p < 0.05$; **, $p < 0.01$; ***, $p < 0.001$, by Student's *t* test.

Figure S5. Localization of NLRP3 and ASC speck.

(A) WT BMDMs were exposed to LPS and subsequently fixed and labelled for NLRP3 and ER marker calreticulin with secondary antibodies conjugated to FITC and Alexa Fluor 546, respectively. Inset and right panel shows zoom of indicated region on the left panel showing merged image. Scale bar, 10 μm **(B)** WT BMDMs were stimulated with LPS and exposed to MitoTracker Deep Red (Alexa fluor 647) during ATP stimulation in OptiMEM media. Subsequently, cells were fixed and labelled for endogenous ASC and ER marker calreticulin with secondary antibodies conjugated to FITC and Alexa Fluor 405, respectively. Inset shows zoom of indicated region on the left panel. Scale bar, 10 μm. Data shown are representative of at least three independent experiments.

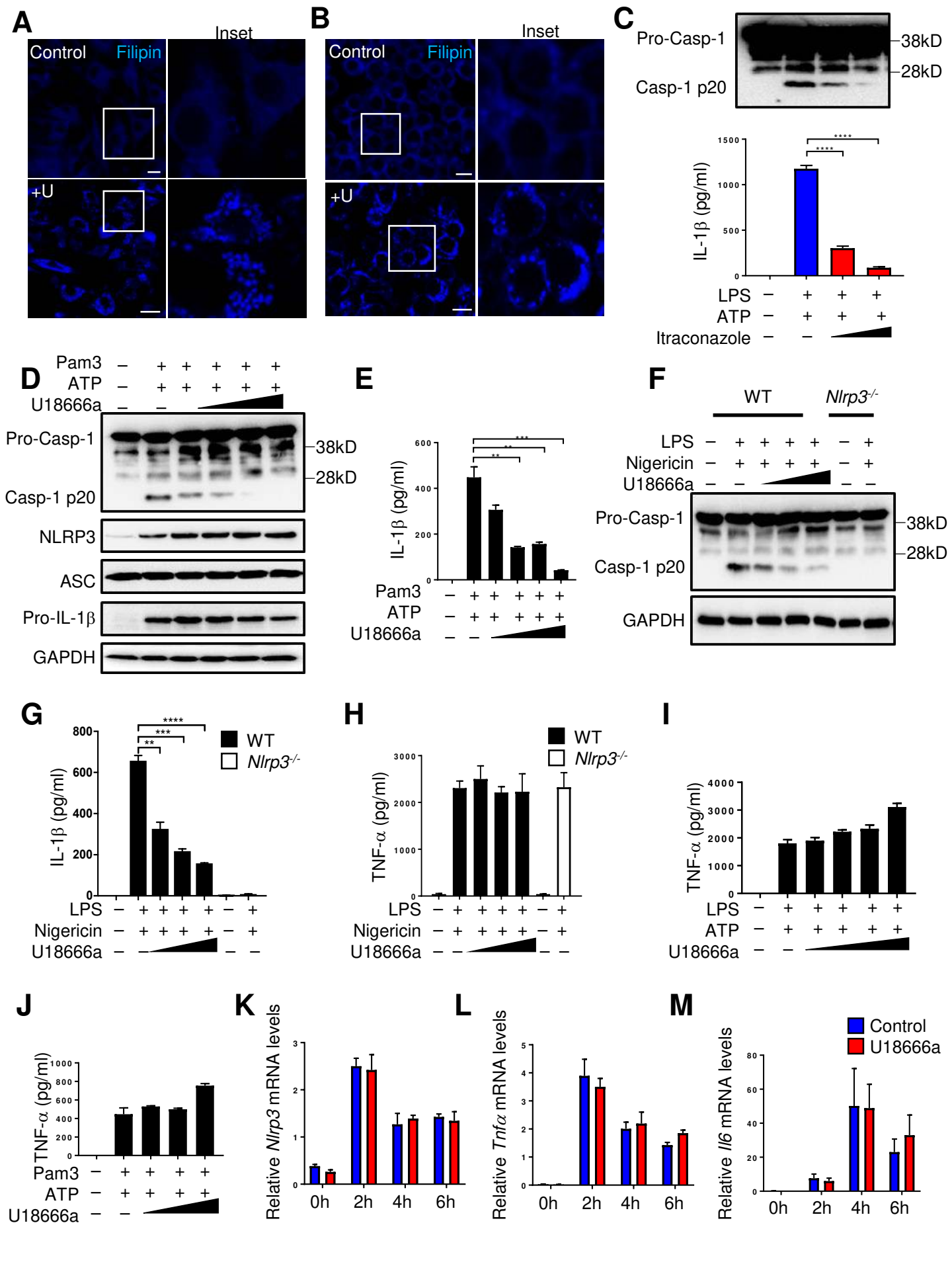
A
Inset
Control
Filipin
+U
B
Inset
Control
Filipin
+U
C
Pro-Casp-1
Casp-1 p20
38kD
28kD
IL-1β (pg/ml)
LPS
ATP
Itraconazole
D
Pam3
ATP
U18666a
Pro-Casp-1
Casp-1 p20
38kD
28kD
NLRP3
ASC
Pro-IL-1β
GAPDH
E
IL-1β (pg/ml)
Pam3
ATP
U18666a
F
WT
Nlrp3-/-
LPS
Nigericin
U18666a
Pro-Casp-1
Casp-1 p20
38kD
28kD
GAPDH
G
WT
Nlrp3-/-
IL-1β (pg/ml)
LPS
Nigericin
U18666a
H
WT
Nlrp3-/-
TNF-α (pg/ml)
LPS
Nigericin
U18666a
I
TNF-α (pg/ml)
LPS
ATP
U18666a
J
TNF-α (pg/ml)
Pam3
ATP
U18666a
K
Relative Nlrp3 mRNA levels
0h
2h
4h
6h
L
Relative Tnfα mRNA levels
0h
2h
4h
6h
M
Control
U18666a
Relative Il6 mRNA levels
0h
2h
4h
6h

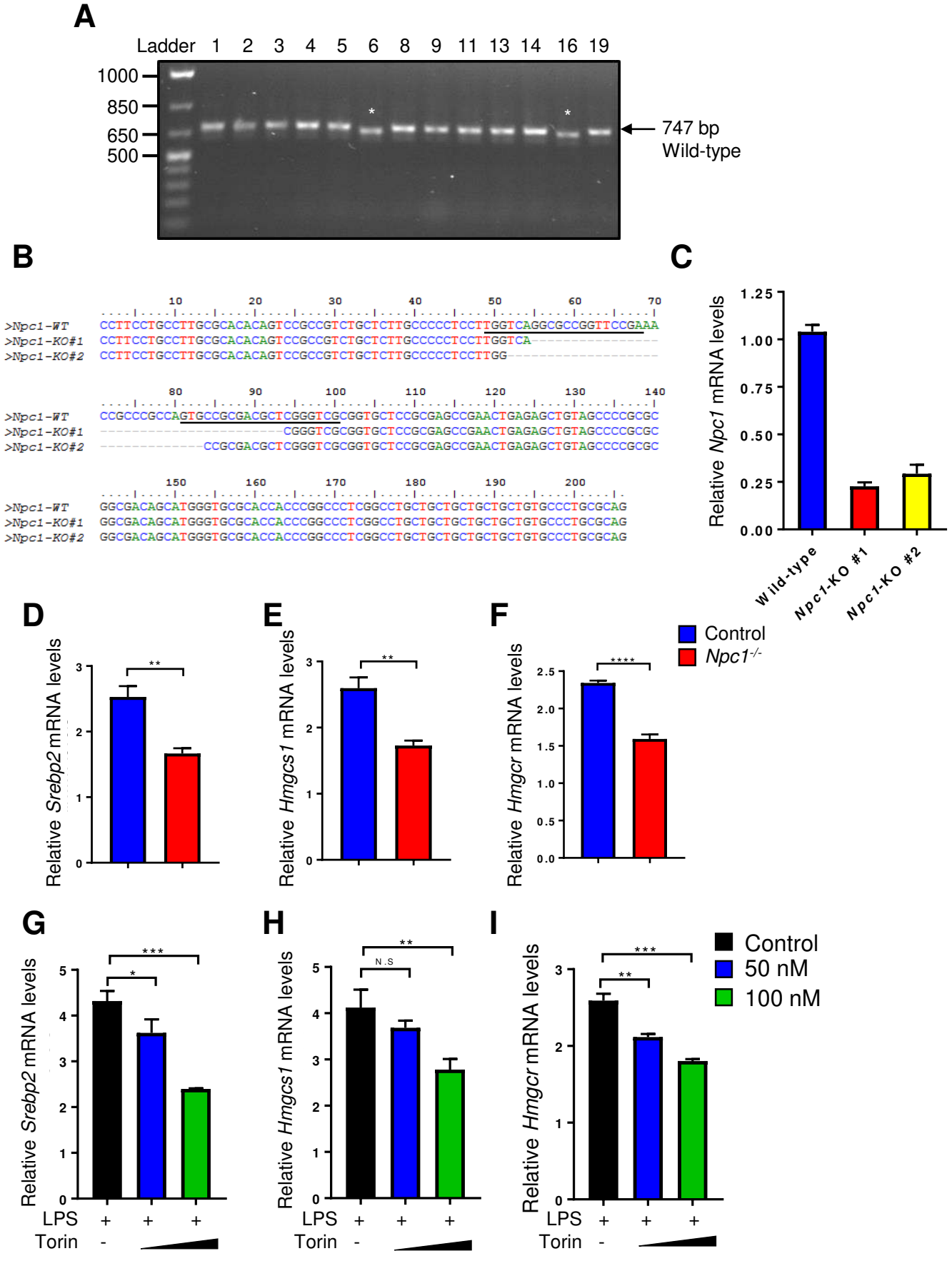
A
Ladder 1 2 3 4 5 6 8 9 11 13 14 16 19
1000
850
650
500
747 bp
Wild-type
B
>Npc1-WT
>Npc1-KO#1
>Npc1-KO#2
C
Relative Npc1 mRNA levels
Wild-type
Npc1-KO #1
Npc1-KO #2
D
Relative Srebp2 mRNA levels
E
Relative Hmgcs1 mRNA levels
F
Relative Hmgcr mRNA levels
Control
Npc1-/-
G
Relative Srebp2 mRNA levels
H
Relative Hmgcs1 mRNA levels
N.S
I
Relative Hmgcr mRNA levels
LPS
Torin
Control
50 nM
100 nM

Figure S2

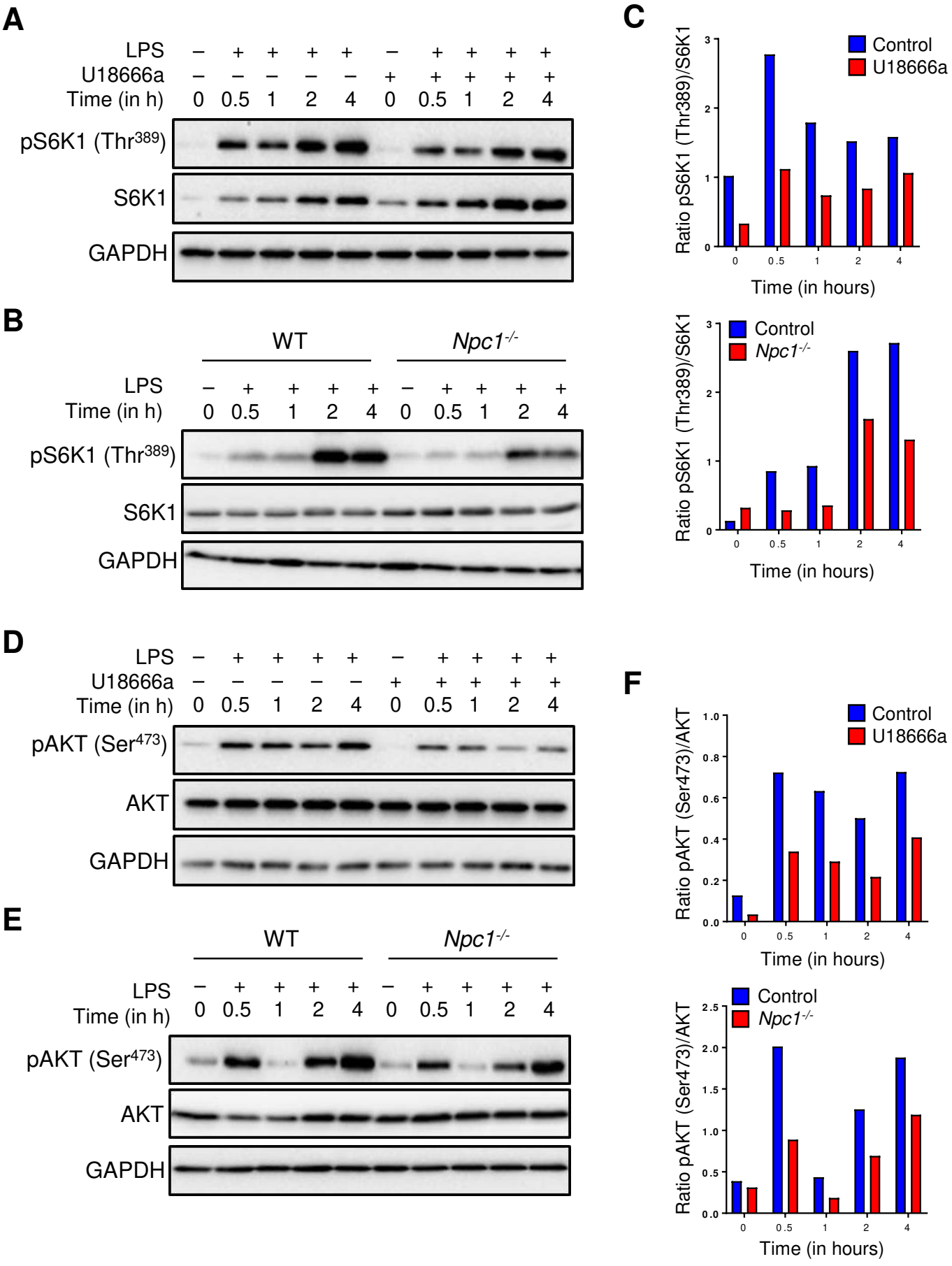
A
LPS
U18666a
Time (in h)
pS6K1 (Thr389)
S6K1
GAPDH
B
WT
Npc1-/-
C
Control
U18666a
Ratio pS6K1 (Thr389)/S6K1
Time (in hours)
D
pAKT (Ser473)
AKT
E
F
Ratio pAKT (Ser473)/AKT

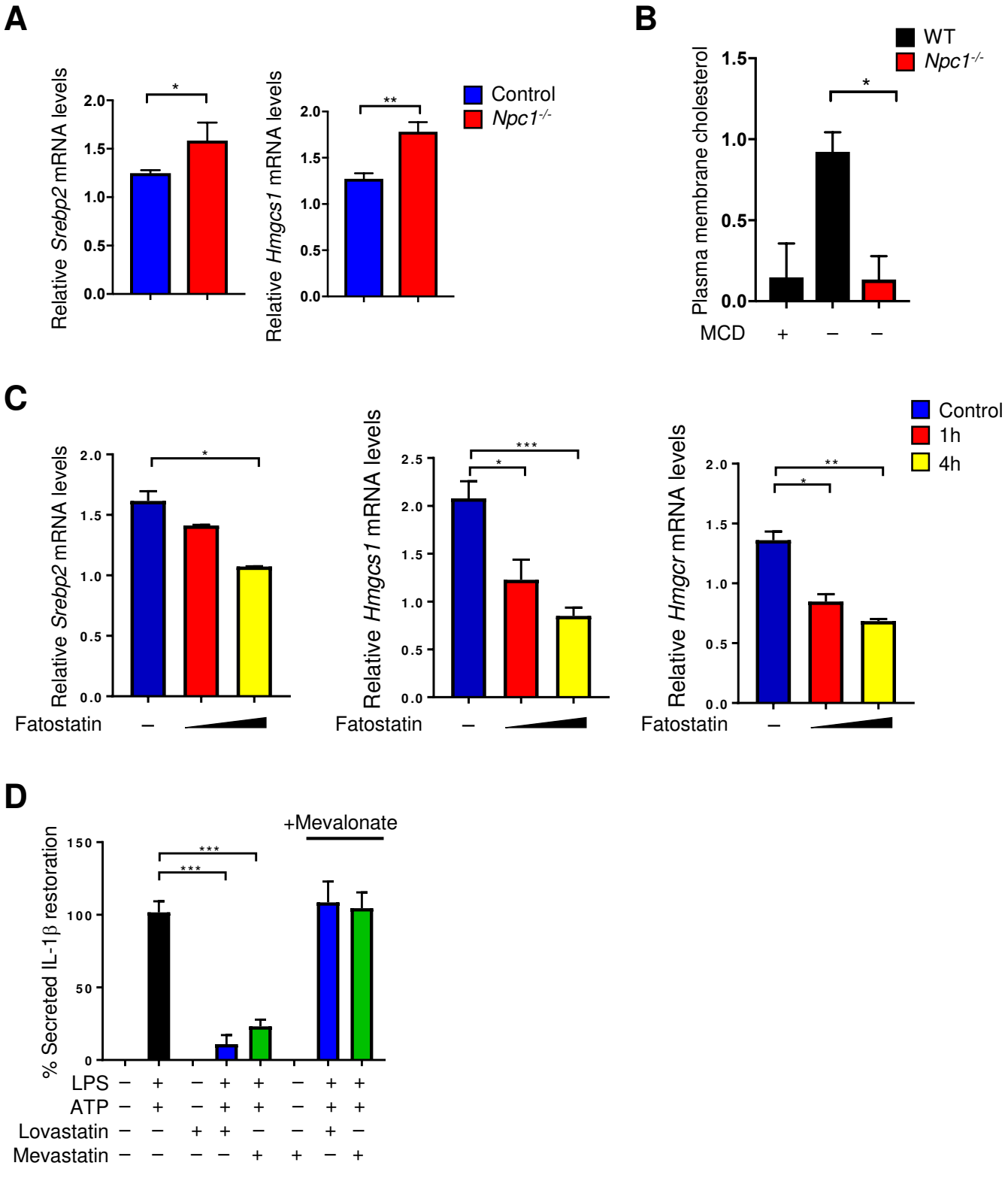
A
Relative Srebp2 mRNA levels
Relative Hmgcs1 mRNA levels
Control
Npc1-/-
B
Plasma membrane cholesterol
WT
Npc1-/-
MCD
C
Relative Srebp2 mRNA levels
Relative Hmgcs1 mRNA levels
Relative Hmgcr mRNA levels
Control
1h
4h
Fatostatin
D
% Secreted IL-1β restoration
+Mevalonate
LPS
ATP
Lovastatin
Mevastatin

Figure S4

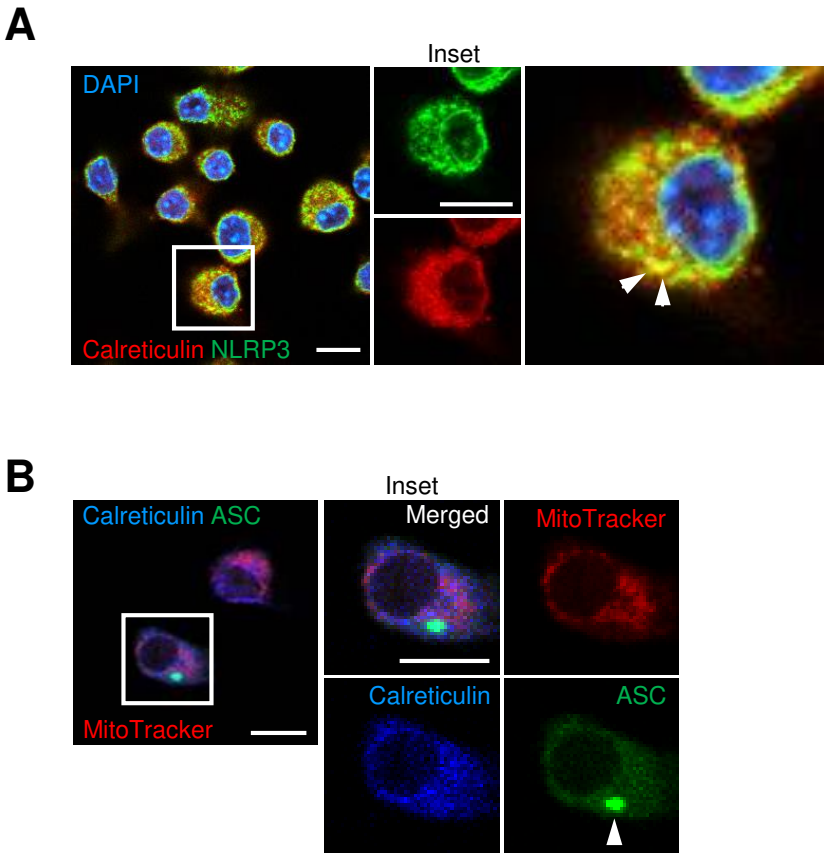
A
Inset
DAPI
Calreticulin NLRP3
B
Inset
Calreticulin ASC
MitoTracker
Merged
MitoTracker
Calreticulin
ASC

Figure S5